The Phase behavior of PS-b-P4VP $(PDP)_x$

Predict the position of the double gyroid morphology in the phase diagram and control its feature size

Thomas Voortman

July 16, 2012

University of Groningen

University of Groningen
Zernike Institute for Advanced Materials

Thomas Voortman
S1762141

Phone: (+31) 621228000
E-mail: thomas.voortman@gmail.com

The Phase behavior of PS-b-P4VP(PDP)$_x$

Predict the position of the double gyroid morphology in the phase diagram and control its feature size

Part of this work was published in: I. Vukovic, **T.P. Voortman**, D.H. Merino, G. Portale, P. Hiekkataipale, J. Ruokolainen, G. ten Brinke, and K. Loos, *Macromolecules* **2012**, *45*, 3503-3512.

Author:

Thomas P. Voortman

Period:

September 2011 – February 2012

Supervisor:

Ivana Vukovic

Institute:

University of Groningen, Zernike institute for advanced materials, Polymer chemistry Prof. Dr. G. ten Brinke and Prof. Dr. K. Loos.

Acknowledgements

The work presented in this master's thesis would not have been possible without the help and support of many people. First of all, I would like to thank my supervisor Ivana Vukovic for her guidance and patience of the last six months. I would not have been able to finish this thesis in time without the good planning capabilities of Ivana and her drive to finish work now and not tomorrow, for that I am very grateful.

Secondly I want to acknowledge Dr. Prof. Gerrit ten Brinke and Dr. Prof. Katja Loos for allowing me to do my research in their group and for their helpful and good suggestions during the group meetings. Of course I also would like to thank all the current and past group members of the Polymer department for their guidance, support and helping me to relax with a freshly (and a bit illegally) brewed espresso. In particular, I would also like to thank Patrick Borgeld personally for the nice atmosphere in our office.

I also want to thank some people from within the polymer department and other groups personally for their help. I want to thank Ryan Chiechi and Parisa Pourhossein for allowing us to use the microtome in their lab and Marc Stuart for allowing us to use the TEM. I also want to show my gratitude to Martin Faber and Vincent Voet for teaching Ivana and me all that we needed to know to operate the high vacuum line and to do the anionic polymerization. Of course I also want to thank Joop Vorenkamp for measuring the molecular weight of our polymers with the GPC and Gert Alberda van Ekenstein for his guidance on the DSC.

Finally I would like to thank my friends, my family, and my girlfriend for their support.

Summary

The gyroid network morphology has been subject of many studies to implement it in a wide range of nano-scale applications. A comprehensive study of the phase behavior of the supramolecular complex of polystyrene-*block*-poly(4-vinylpyridine) (PS-*b*-P4VP) mixed with 3-pentadecylphenol (PDP) was conducted, in order to develop a simple route to its double gyroid network morphology. Films were prepared from a wide range of PS-*b*-P4VP compositions and PDP concentrations. Our approach does not require time consuming syntheses of block copolymers (BCPs) with several compositions in search for different morphologies; by simply increasing or decreasing the PDP concentration to a specific PS-*b*-P4VP BCP, the morphology can be altered. PDP can be removed by immersion in ethanol resulting in the collapse of the P4VP chains onto the PS phase to produce nanoporous polymer templates. Analysis of the morphologies by transmission electron microscopy (TEM) and small angle X-ray scattering (SAXS) revealed that with increasing volume fraction of the comb block, first lamellae, then gyroid, and finally cylinders are found. Furthermore, the gyroid region contracts with increasing degree of polymerization (*N*) of the starting BCP and above a critical value the gyroid morphology is no longer observed. Biphasic morphologies were also observed where the gyroid morphology was found along with lamellae or cylinders. By selecting BCPs with a different molecular weight the lattice parameter of the gyroid morphology could be ranged from 71 nm to 127 nm. Furthermore, the gyroid morphology was obtained for different concentrations of PDP, thus, a range of porosities can be chosen after dissolution of PDP. Analysis by DSC of mixtures of PS-*b*-P4VP with PDP and polystyrene mixed with PDP indicated that, although PDP can migrate into the PS phase, its concentration in the PS phase of the BCP probably remains below 1 wt%. The BCP we used are commercially available, however, we ran out of material of a specific sample and could not order it anymore. Therefore, we used the anionic polymerization technique to synthesize this BCP. Unfortunately, we have not been able to synthesize the BCP with the required composition as was determined by proton nuclear magnetic resonance (^{1}H-NMR) and gel permeation chromatography (GPC). Future work could include back-filling of an empty gyroid template with an inorganic material, for instance, metal alloy by electroless plating in order to achieve a hierarchically porous nanofoam, after etching away the polymer and the less noble metal.

Contents

ACKNOWLEDGEMENTS ..... **II**

SUMMARY ..... **III**

1. INTRODUCTION **1**

1.1. POLYMER MISCIBILITY 2

1.2. BLOCK COPOLYMER SELF-ASSEMBLY 3

1.3. SUPRAMOLECULAR COMPLEXES 6

1.4. THE BICONTINUOUS GYROID MORPHOLOGY AND ITS APPLICATIONS 8

1.5. METAL NANOFOAMS 9

1.6. NANO-SCALE STRUCTURES IN NATURE 12

1.7. REFERENCES 14

2. RESULTS AND DISCUSSION **17**

2.1. THE PHASE DIAGRAM OF PS-B-P4VP(PDP)$_x$ 17

2.1.1. Sample preparation method *18*

2.1.2. Morphological study by transmission electron microscopy *20*

2.1.3. Morphological study by small angle x-ray scattering *23*

2.1.4. Tunable polymer template porosity *28*

2.2. THE POSITION OF PDP IN THE COMPLEX 30

2.2.1. The glass-transition temperature of PS in PS-b-P4VP mixed with PDP *31*

2.2.2. The glass-transition temperature of PS in PS homopolymer mixed with PDP *33*

2.3. ANIONIC POLYMERIZATION OF PS-B-P4VP 36

2.4. REFERENCES 43

3. CONCLUSIONS **45**

4. EXPERIMENTAL SECTION **46**

4.1. MATERIALS 46

4.2. FILM PREPARATION 46

4.3. CHARACTERIZATION 46

4.4. SYNTHESIS 47

4.5. REFERENCES 48

1. Introduction

This master's thesis describes the investigation of the phase behavior of a polystyrene-*block*-poly(4-vinylpyridine) (PS-*b*-P4VP) block copolymer (BCP) mixed with 3-pentadecylphenol (PDP). When the amphiphile PDP is added to poly(4-vinylpyridine) (P4VP) hydrogen-bonds are formed between the nitrogen of the pyridine ring and the hydrogen of the phenol ring. The result is a comb–coil block copolymer with an increased volume fraction of the P4VP, i.e., P4VP(PDP), block. By varying the amount of added PDP, the fraction of a comb block P4VP(PDP) (and the interaction parameter χ) is altered which allows the control of the phase behavior of the system. Therefore, by varying the amounts of PDP relative to P4VP we can move horizontally in the phase diagram and by changing the total molar mass of the starting BCP we can move vertically in the phase diagram. This strategy does not require time consuming syntheses of BCPs with several compositions in search for different morphologies; by simply increasing or decreasing the PDP concentration to a specific PS-*b*-P4VP BCP, the morphology can be altered. PDP can be selectively removed by soaking a film in ethanol and the resulting porosity of the polymer template is dependent of the original volume fraction of PDP in the complex. Furthermore, by selecting starting BCPs with different compositions that generate the gyroid morphology after mixing with PDP, the porosity of metal nanofoams, which can be generated from these films after pyrolysis of the polymer, can be chosen. We prepared a series of films with a wide range of PDP concentrations and BCP compositions and studied the bulk morphologies with transmission electron microscopy (TEM) and small angle x-ray scattering (SAXS). Because PDP plays a key role in the phase behavior of PS-*b*-P4VP(PDP)$_x$, we also investigated the effects of PDP to the T_gs of each block in order to elucidate the position of PDP in the complex by means of differential scanning calorimetry (DSC). The majority of the BCPs we used in this master's thesis were commercially available, however, since supplies are limited and a specific BCP composition was not available anymore, we used the living anionic polymerization technique to synthesize this particular BCP.

1.1. Polymer miscibility

Polymers consist of a large number of low molecular weight units or monomers that are covalently linked together to form a long chain. The most straightforward example of a synthetic polymer is polyethylene (i.e., $-(CH_2-CH_2)_n-$). Chemically distinct polymers generally do not mix in the melt state and separate into different layers—in a similar fashion that oil and water do not mix—and this process is called macrophase separation. A two component system will spontaneously mix if the change in the (Gibbs) free energy of mixing (ΔG_m) is negative: $\Delta G_m = \Delta H_m - T\Delta S_m$ (N.B., in polymer mixtures the free energy of mixing is often negative but phase separation lowers G_m even more). The change in the Gibbs free energy of mixing is defined by the change in the interaction energy upon mixing, given by the enthalpy of mixing (ΔH_m), and the change in entropy upon mixing (ΔS_m) at a certain temperature (T). If we consider a mixture of two chemically distinct polymers with a degree of polymerization N_1 and N_2 and if we divide the polymer chains in segments that occupy the same volume per segment (i.e., in the lattice model), we can express the Gibbs free energy by the so called Flory-Huggins theory[1]:

$$\frac{\Delta G_m}{nkT} = \frac{\varphi}{N_1}\ln\varphi_1 + \frac{\varphi}{N_2}\ln\varphi_2 + \chi\varphi_1\varphi_2 \qquad (1)$$

here n represents the number of segments, k the Boltzmann constant, φ the volume fraction, and χ the Flory-Huggins interaction parameter defined as $\chi = z/kT\,[\varepsilon_{12} - ((\varepsilon_{11} + \varepsilon_{22})/2)]$ with z the lattice coordination number (i.e., the number of nearest neighbors) and ε the interaction energy between different segments. The first two terms of equation 1 describe the change in the entropy of mixing and the third term gives the change in the enthalpy upon mixing the polymer with a degree of polymerization of N_1 with the polymer with a degree of polymerization of N_2 (N.B., the degree of polymerization is expressed here in terms of the number of segments, not monomer units). The critical values of the volume fraction and the χ-parameter mark the points at which just no macrophase separation occurs and are found at $\varphi_c = \sqrt{N_2}/(\sqrt{N_1} + \sqrt{N_2})$ and $\chi_c = 1/2\left(1/\sqrt{N_1} + 1/\sqrt{N_2}\right)^2$, respectively. When $N_1 = N_2 = N$ we find that $\varphi_c = 1/2$ and $\chi_c = 2/N$ and since N is generally very large for polymers the critical value of the Flory-Huggins interaction parameter is very small. This means that already at very small positive values of the χ-parameter macrophase separation occurs.[2]

1.2. Block copolymer self-assembly

A block copolymer (BCP) consists of two or more chemically different homopolymers covalently linked end-to-end and because of this linkage they cannot macrophase separate. However, due to the unfavorable interactions between the different blocks phase separation still occurs but, because of their connectivity, only on the nanometer scale and this process is called microphase separation. The way that BCPs self-assemble into periodic nanostructures has been poetically described by Helfand and Wasserman[3]: "Like a child contemplating the result of tying the cat's tail to that of a dog, scientists perhaps find a certain mischievous delight in considering the effect of joining two immiscible polymer blocks into one macromolecule. The immiscible units attempt to separate, but by virtue of their connectivity they can never get very far from each other. The result is that they either segregate into micro-domains or remain homogeneously mixed with each other." The phase separation in BCPs is driven by two opposing forces: the unfavorable interactions between chemically distinct species induce stretching of the polymer chains (i.e., to minimize the interaction enthalpy) and the entropic elasticity (of the entropic spring) resists this stretching (i.e., to maximize the conformational entropy). If the polymer chains are fully stretched there are less unfavorable interactions but the number of possible conformations is reduced to one. It, thus, depends on the temperature and the strength of the interactions which tendency is dominant. At high temperatures the entropic factor is large and the BCP becomes homogenously mixed. When the temperature drops below a certain value, the enthalpic contribution becomes dominant and causes the BCP to microphase separate. The manner of microphase separation is dependent of the composition of the BCP (i.e., the degree of polymerization of each block); changing the volume fraction of one of the blocks can lead to a range of different ordered-phase symmetries. In Figure 1 the schematic illustrations of some of the most common (classical) and complex phases are depicted, showing the domains of the minority phase. In the blow-up of the lamellar morphology the self- assembly of individual molecules within the domains is shown where the blue and red parts represent the two chemically distinct blocks.[14] Experimentally it has been demonstrated that in the case of nearly monodisperse polyisoprene-polystyrene (PI-*b*-PS) for $0.24 < f_{PI} < 0.82$ spheres (SPH), cylinders (CYL), hexagonally perforated layers (HPL) (which is actually a metastable phase[5a]), bicontinuous gyroid

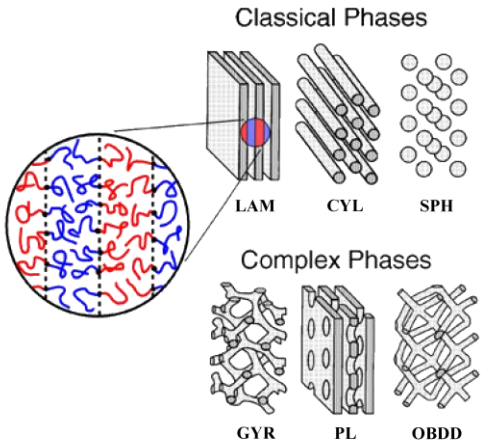

Figure 1. *Schematic representations of six ordered morphologies showing only the domains of the minority phase (i.e., with the shortest chain length) and the blowup of the LAM phase shows the self-assembly of individual BCP chains within this morphology. The lamellar (LAM), cylindrical (CYL) and the spherical (SPH) morphologies are three examples of the most common, classical phases and the gyroid (GYR), perforated lamellar (PL), and the ordered bicontinuous double-diamond (OBDD) are three examples of the more complex morphologies known in diblock copolymers.*[14]

(GYR), and lamellae (LAM) can be observed.[4] There are numerous copolymer architectures known but the simplest examples are linear diblock copolymers. Linear triblock copolymers and multiblock copolymers can form the classical morphologies but also complex structure-within-structure morphologies.[5] More complex polymer architectures have also been studied such as branched, grafted, and star copolymers. Dependent on the composition, grafted copolymers can also form the classical morphologies.[6] Star-shaped copolymers are triblock or multiblock copolymers that are connected to a single point and this architecture results in Archimedean tiling pattern morphologies that are unique to this type of copolymers.[7]

The phase behavior of BCPs can be described in the strong segregation limit[8] (SSL), where the product $\chi N >> 10$, and in the weak segregation limit[9] (WSL) where $\chi N \lesssim 10$ (here N denotes the number of monomer units in the polymer chain). The theories describing the SSL assume relatively sharp interfaces and chain stretching. In the case of the WSL the interfaces are rather "sinusoidal" and chain stretching is neglected. By using the self-consistent field theory (SCFT)[10] Matsen and Bates calculated the phase diagram of diblock copolymers in the mean field phase[11] (i.e., in between the SSL and the WSL) which is shown in Figure 2 along with the representations of the corresponding morphologies. Although theory provides us with a fundamental understanding and intuitive explan-

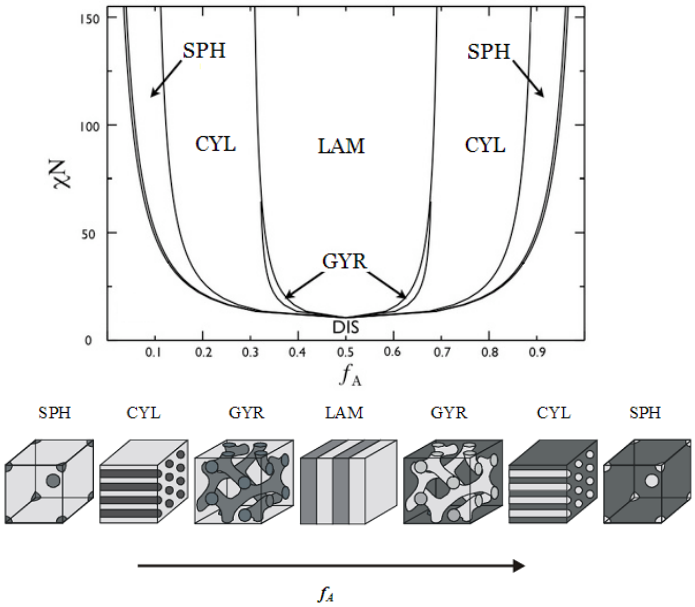

Figure 2. *The phase diagram as calculated by Matsen and Bates for a conformational symmetric diblock melt in the mean field segregation showing some of the most commonly known morphologies: spheres (SPH), cylinders (CYL), lamellae (LAM), and gyroid (GYR)*[11] *and below the phase diagram the corresponding representations of the different morphologies are shown.*[12]

ations of the phase behavior of BCPs, experimental phase diagrams are usually quite different from theoretical phase diagrams (see reference 14). Fluctuation effects that are not included in the mean-field calculations and asymmetries in the statistical segment length of each block can explain some dissimilarity. Furthermore, the experimental errors (i.e., non-equilibrium effects, uncertainties in molecular weight characteristics, impurities, *etc*.) should also be considered when discussing the differences between experimental and theoretical phase diagrams.[13,14]

A specific example of a diblock copolymer that is of interest for this master's thesis is the polystyrene-*block*-poly(4-vinylpyridine) (PS-*b*-P4VP) block copolymer. The microphase separation of PS-*b*-P4VP in bulk as well as in thin films has been widely explored in literature. For example, it has been shown that the morphology of PS-*b*-P4VP thin films can be tuned by using different solvents.[15] It was also demonstrated that PS-*b*-P4VP can be applied as thin films with a pH-responsive wettability.[16] In other recent publications it has also been demonstrated that the PS-*b*-P4VP BCP can be used as a good candidate for nanopatterning[17] and non-solvent-induced phase separation[18] for membrane development or highly ordered quantum dot arrays.[19] Other uses of PS-*b*-P4VP include cylindrical gate insulators in thin film transistors[20], composite nanostructured arrays[21], and hollow capsules.[22]

1.3. Supramolecular complexes

Supramolecular complexes are chemical compounds (usually with a high complexity) that are build-up and held together by intermolecular, non-covalent binding interactions.[23] A specific example of a supramolecular complex is that of a comb-block copolymer (i.e., a BCP that contains side chains or branches on one or more blocks) in which the side chains are not chemically linked, but physically complexed via hydrogen-bonding. The supramolecular complexes of P4VP with PDP, PS-*b*-P4VP with PDP, and similar systems are extensively studied in our group.[24] Each PDP molecule contains a hydroxyl group which acts as a hydrogen-bond promoting group and each repeat unit of P4VP contains a nitrogen atom that can act as a hydrogen-bond accepting group. Therefore, if PDP is added to P4VP, hydrogen-bonds are formed between the nitrogen of the pyridine ring and the hydrogen on the phenol ring.[25] The chemical structure of PDP hydrogen-bonded to PS-*b*-P4VP is drawn in Figure 3. Ruokolainen *et al.* suggested that the a-polar tails of PDP microphase separate from P4VP in such a way that the PDP molecules align perpendicular to the P4VP homopolymer (Figure 3). Furthermore, they also claimed that by changing the ratio of PDP molecules relative to the number of 4VP units different lamellar layer thicknesses can be obtained and demonstrated this effect by SAXS.[25] In later work Ruokolainen *et al.* showed that when PDP is complexed to PS-*b*-P4VP, two length scale ordering appears in the form of lamellar-within-lamellar structures.[26] By either changing the BCP composition or the PDP concentration they found spherical, cylindrical, and lamellar morphologies by TEM and SAXS analysis.[27] Furthermore, they demonstrated the temperature dependence of the Hydrogen-bonding of PDP with P4VP.[28] In the following years the phase diagram of PS-*b*-P4VP(PDP)$_{1.0}$ (the subscript denotes the ratio of PDP relative to the 4VP units) was investigated, at room temperature and at elevated temperatures, and all classical morphologies—but also more complex structures-within-structures—were found.[29] The Flory-Huggins χ-parameter between PS and P4VP was studied comprehensively by a random-block copolymer miscibility study and it was determined to be 0.34. This meant that PS-*b*-P4VP is in the strong segregation regime, except for very small molar masses.[30] Polushkin *et al.*[31] investigated the chain length dependence of the long period in the microdomain structures of supramolecular complexes. The long period, *D*, of a lamellar microdomain structure is dependent on the chain length *N* and in the SSL the long period scales as $D \sim N^{0.67}$. Via a SAXS study

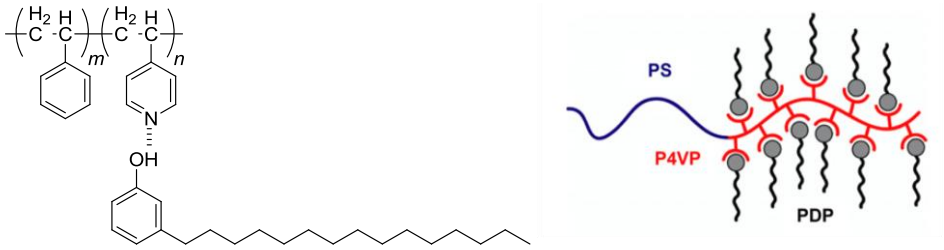

Figure 3. *The chemical structure of poly(styrene-b-4-vinylpyridine) (PS-b-P4VP) showing the hydrogen-bond between the hydroxyl group of 3-pentadecylphenol (PDP) and the nitrogen of the pyridine ring of 4-vinylpyridine on the left and on the right a schematic representation of PS-b-P4VP(PDP).*

of multiple PS-*b*-P4VP compositions, a scaling exponent of 0.7 was found which confirmed the assumption that this BCP is in the strong segregation regime. Next, they mixed PDP in different concentrations to PS-*b*-P4VP and measured the long period of lamellar morphologies by SAXS and found the scaling exponent for different samples to be 0.81 ± 0.04, 0.83 ± 0.04, and 0.84 ± 0.04. These values are close to the scaling exponent values of the intermediate segregation regime where $D \sim N^{0.8}$. The authors concluded that the system is in the intermediate segregation regime because part of the PDP molecules diffuses into the PS layers, where they accumulate at the interfaces, resulting in lower interfacial tensions and a diffuse interface. The phase behavior of the supramolecular complex of PDP with PS-*b*-P4VP was also investigated in thin films by *Zoelen et al.*. By applying vapor annealing, a film thickness dependent morphology with sharply defined boundaries, in a terrace architecture with different heights, was found.[32] The investigation of the supramolecular complex of PDP with P4VP was also extended to triblock copolymers for poly(tert-butoxystyrene)-*b*-polystyrene-*b*-poly(4vinylpyridine) by Gobius du Sart and coworkers. They found a core-shell gyroid morphology of which the core consisted of hydrogen-bonded P4VP(PDP) complexes. By immersion in ethanol they were able to remove PDP resulting in well-ordered nanoporous films that could be used as templates for nickel plating. [33,34]

In the literature there are several recent publications to be found regarding similar research on supramolecular complexes. For instance, a research group from Taiwan investigated the PS-*b*-P4VP(PDP)$_x$ in thin films and found either lamellae or cylinders parallel or perpendicular to the surface by varying the concentration of PDP to PS(20000)-*b*-P4VP(17000) or PS(40000)-*b*-P4VP(5600).[35] Ikkala and coworkers replaced PDP by cholesteryl hemisuccinate (CholHS) that can from hydrogen-bonds via

an acid group and observed similar phase behavior to that of PDP. They mixed CholHS with P4VP homopolymer, to generate a liquid crystal, and with PS-*b*-P4VP to allow hierarchical structure-within-structure self-assembly.[36] Another group from Leibniz Institute of Polymer Research mixed 1-pyrenebutyric acid (PBA) amphiphiles to PS-*b*-P4VP and generated thin films. They found that the cylindrical morphology of the pure BCP changes to a lamellar morphology with an increase in the comb volume fraction. They also used ethanol immersion to selectively remove PBA in order to generate nanotemplates for the fabrication of arrays of nanowires.[37] Wang *et al.* mixed PS-*b*-P4VP with poly(4,4'-oxydiphenyl-enepyromellitamic acid) (POAA) where each repeat unit of POAA can from hydrogen-bonds with two 4VP units. They found ordered microphase-separated structures of spherical PS domains in a P4VP/POAA matrix after solvent annealing in a benzene/NMP mixture.[38]

1.4. The bicontinuous gyroid morphology and its applications

Meuler, in collaboration with Hillmyer and Bates, wrote an elaborate review article regarding ordered network mesostructures in BCPs. They summarized experimental and theoretical investigations of the structures and properties of these network morphologies in AB and ABC BCP systems.[39] In 1976 it was noted that bicontinuous geometries have less interfacial area than structures of discrete spheres. Because of the thermodynamic driving force to minimize interfacial area, continuous networks are formed.[40] The term "ordered bicontinuous structure" was first used in 1986 by Alward and coworkers.[41] Schoen calculated 17 of these bicontinuous networks and labeled the minimal surface structure, to describe the $Ia\bar{3}d$ symmetry, by the name "gyroid" (GYR).[42] The gyroid network is a unique morphology because both the network phase and its matrix phase are continuous throughout the bulk of the material.[43] Due to the connectivity of both of the phases, and the nanometer size struts, the bicontinuous gyroid morphology has been used in a wide range of applications: as precursors for metal nanofoams, photonic crystals, hybrid solar cells, antireflection structures, catalysts, ceramic membranes, and membrane reactors.[44]

The region of the volume fraction *f* where the gyroid morphology can be observed is narrow and it contracts with increasing χN[45] and, therefore, the length of the blocks and the monomers need to be carefully chosen in order to obtain the gyroid morphology. Recently, a supramolecular route to

well-ordered metal nanofoams was proposed by Vukovic and coworkers.[46] They used PS-*b*-P4VP(PDP) with a gyroid morphology and—similarly as in the triblock system—PDP could be removed by immersion in ethanol to generate a nanoporous template. Via electroless nickel plating the template was backfilled with metal and after pyrolysis an inverse gyroid nickel nanofoam was obtained. This paper forms the basis of this master's thesis and we will try to extend it by a complete investigation of the phase diagram of PS-*b*-P4VP(PDP)$_x$. By varying the amount of added PDP and/or the total molar mass of the PS-*b*-P4VP block copolymer we can move horizontally and vertically in the phase diagram of the BCP, respectively. This approach does not require time consuming synthesis of BCPs with different compositions in search for the double gyroid morphology; by simply increasing or decreasing the PDP concentration, to a specific PS-*b*-P4VP BCP, different morphologies can be obtained. With the correct parameters we obtain a bicontinuous gyroid morphology with a minority PS phase embedded in a P4VP(PDP)$_x$ matrix. PDP can then be selectively removed by dissolution in a selective solvent which leaves the PS phase unchanged. Because the P4VP chains are "supported" by the PDP molecules, they collapse onto PS when PDP is removed, thus creating a P4VP corona around the PS network struts. The result of this investigation can be found in section 2.1. In this master's thesis we are also interested in the position of PDP in the complex because it has been demonstrated earlier that PDP can mix with PS (section 2.2). We also synthesize a specific BCP via the living anionic polymerization in order to complete a specific part of the phase diagram as we will discuss in section 2.3. Furthermore, in this master's thesis we review literature regarding plating processes in the next paragraph.

1.5. Metal nanofoams

A nanofoam represents a porous material with a pore size in the nanometer scale and it can be used, e.g., as a template for nanofabrication. Templates generated from perpendicular ordered hexagonally packed cylinders generally require costly and time consuming alignment procedures. In contrast, the bicontinuous gyroid network can be obtained without the need of alignment steps.[39] Several strategies have been reported in literature to selectively remove one of the blocks of a BCP to generate a porous template. For example, Hsueh *et al.* removed the lactide network phase of the

gyroid morphology of polystyrene-*b*-poly(L-lactide) (PS-*b*-PLLA) by hydrolysis. They next templated the empty gyroid with silica and after subsequent UV-degradation of the PS matrix they obtained a silica nanofoam.[44a] Similarly, PI has been removed by UV radiation from a PI-*b*-PS gyroid film to generate a (nonmetallic) photonic crystal. [44c]

Electroplating and electroless plating are two of the most commonly used techniques for the deposition of metals onto or into templates. In electroplating metal ions are reduced to the metallic state and then deposited at the cathode by means of electrical energy. In the case of electroless plating a metal is deposited via a chemical reduction process on a substrate without the use of electrical energy.[47] The discovery of electroless plating is generally credited to Brenner and Riddell[48], however, the use of sodium hypophosphite, as a reducing agent, to produce electroless nickel coatings was first observed by Wurtz in 1844.[49] The advantage of electroless plating over electroplating, is that coatings generated via the electroless procedure always have uniform thicknesses and constant mechanical properties; a combination that is hard to achieve with electroplating techniques. The baths in which electroless plating takes place are often very complex and contain multiple components. A typical electroless plating bath consists of: (i) metal ions, (ii) reducing agent that are in a metastable equilibrium with the metal ions, (iii) complexants to prevent excess free metal ions, precipitation, and, in some cases, also acts as pH buffer, (iv) accelerators to speed-up the deposition, (v) stabilizers to prevent solution breakdown, (vi) buffers for long term pH regulation, (vii) pH regulators to subsequently adjust the pH of the solution, and (viii) wetting agents to increase the wettability of the substrate.[50] Electroless plating is also possible for non-conducting substrates such as polymer films, however, two additional steps are required: firstly the surface needs to be sensitized and secondly an activation step is required. The sensitization step involves the immersion of the template in stannous chloride-hydrochloric acid in order to deposit tin hydrosol particles on the surface. To activate the surface the template is next immersed in an acidified palladium chloride solution in which, via a redox reaction, seed crystals of metallic palladium are formed that act as catalyst for the electroless plating of metal.[50b]

In the literature some publications can be found that use metal plating techniques to back-fill emptied gyroid films. For example, Hashimoto *et al.* used a gyroid morphology of PI-*b*-PS and

removed PI by ozone degradation. They then used electroless plating to back-fill the empty PS gyroid film with nickel.[51] The electroless plating of nickel was also implemented on PS-*b*-PLLA films with the gyroid morphology by Hsueh *et al.* and they successfully obtained a nickel nanofoam.[52] However, these authors do not show the penetration depth of the metal in the polymer templates. Crossland *et al.* showed that films of poly(4-fluorostyrene)-*b*-poly(D,L-lactide) (PFS-*b*-PLA), that have a gyroid morphology, can be used to generate a porous template by hydrolysis of PLA. They used the electrochemical deposition of TiO_2 to replicate the gyroid morphology and subsequently degraded the PFS matrix phase. This TiO_2 could then be used for the fabrication of a solid-state-dye sensitized solar cell.[53]

Electroless plating is thoroughly addressed in "*Electroless Plating: Fundamentals And Applications*" and also the deposition of different metal alloys are briefly discussed in chapter 15.[54] In 2010 the book "*Modern Electroplating, Fifth Edition*" was published which also shortly addressed the possibilities of electroless metal alloy deposition.[55] A homogeneous gold-silver alloy can be obtained by using a borohydride gold bath with continuous addition of $KAg(CN)_2$ and excess free cyanide. The continuous addition is required for a uniform alloy deposit because the silver complex is much more readily reduced than the gold complex. Another possibility is the gold-copper alloy that can be plated with a tunable gold/copper ratio (5 to >99.5% gold) by adding a certain amount of $Au(CN)_2^-$ to a conventional electroless copper plating bath (containing copper sulfate, potassium cyanoaurate) with EDTA and formaldehyde. In this alloy plating procedure copper acts as a catalyst for the oxidation of formaldehyde to facilitate the plating of both copper and gold. Gold-copper alloys can also be deposited by electroplating, however, these alloys consist of partly individual metal crystals and gold-copper mixed crystals. In contrasts, the alloys obtained via the electroless alloy plating procedure contain homogeneously mixed metal crystals. A third described alloy is a gold-tin alloy which is obtained from an electroless gold plating bath containing stannous chloride (as the reducing agent). The tin content of the alloy was also varied between 5 and 60%.

In the supramolecular route to well-ordered metal nanofoams proposed by Vukovic *et al.*[46] nickel was used to back fill a porous gyroid template. One idea in our group is to back-fill a gyroid porous template with a metal alloy so that we are, theoretically, able to obtain a hierarchical porous

Table 1. *The composition and reaction conditions of an electroless gold-copper alloy plating bath.*[54]

Ingredient/ Condition	Concentration
$CuSO_4 \cdot 5H_2O$	0.04M
Na_4EDTA	0.072M
NaOH	0.12M
$KAu(CN)_2$	x M (See Table 2)
KCN	0.0015M
Formaldehyde	0.10M
Temperature	50 ˚C

Table 2. *Compositions and quantities of deposited alloys at various gold concentrations.*[54]

$KAu(CN)_2$ (x M)	Deposited alloy in 2h (mg/cm^2)	Au (wt%)	Cu (wt%)
0.00017	2.5	5.8	94.2
0.00035	2.8	7.4	92.6
0.00087	3.1	17.4	82.7
0.0017	3.6	48.3	51.7
0.0035	4.5	65.0	35.0
0.007	2.7 (1h)	74.9	25.1
0.014	2.3	99.0	1.0

metal nanofoam after selectively etching away the less noble metal. For example, if we are able to back fill the gyroid porous template with a gold/copper alloy, and selectively etch away copper with a nitric acid/hydrochloric acid mixture, we can obtain an inverted gyroid gold nanofoam with randomly distributed nanopores within the gyroid struts. Many different metal alloys have been electroless plated but most are nickel-based alloys containing iron, rhenium, molybdenum, tungsten, zinc, tin, or copper.[55] However, to the best of our knowledge, there are no recent publications covering the use of metal alloys on polymer templates and, therefore, precise formulations of plating baths are incomplete or not available at all. Many alloy electroless plating procedures are based on the conventional plating baths of one of the metals and the ion source of the other metal is added. After sensitization and activation of a porous polymer template it might be the case that the electroless plating of an alloy works as well as the electroless deposition of a single metal. An example of an electroless gold-copper alloy plating bath at various gold ratios is given in Table 1 and Table 2.

1.6. Nano-scale structures in nature

Above we discussed the phase behavior of polymer mixtures, BCPs and of supramolecular complexes. In the last century our understanding of the physical explanations of this phase behavior

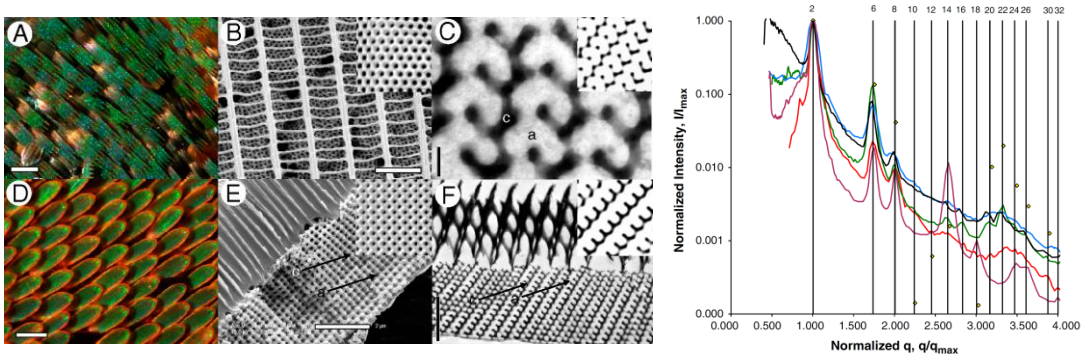

Figure 4. *Anatomy of the structural color-producing nanostructures in lycaenid and papilionid butterflies with (A) and (D) Light micrograph images, (B) and (E) SEM images, and (C) and (F) TEM images. Also shown are the SAXS scattering patterns of the nanostructures of five butterfly species that contain a gyroid morphology as indicated by the peaks 6 and 8 and higher scattering peaks.*[56]

has strongly increased. Synthetic materials are used to investigate the full range of the phase diagrams to generate nano-scale phase separation into well-ordered structures for diverse applications. However, nature has found a way to use self-assembly in a very precise and remarkable fashion to generate color. In particular, the scales of papilionid and lycaenid butterflies consists of three-dimensional complex networks that make-up the photonic crystals to generate color by means of reflection in visible wavelengths. Saranathana *et al.*[56] investigated five butterfly species by SAXS, scanning electron microscopy (SEM), and TEM and wrote: "After millions of years of selection for a consistent optical function, photonic crystals in butterfly wing scales are an ideal source to inspire biomimetic (i.e., bio-inspired) technology. Indeed, their optical properties have at times surpassed those of engineered solutions." In Figure 4 the anatomy of the structural color-producing nanostructures in lycaenid and papilionid butterflies is shown by light microscopy, SEM, and TEM analysis. By SAXS analysis the authors observed a large number of spots and because of the irregular angles between these spots they concluded that there are a number of distinctly oriented crystallite domains present in the scales of these butterflies. Furthermore, they concluded, based on the scattering patterns and SEM and TEM results, that all five butterfly species have perfect gyroid morphology as the structural color-producing nanostructures. It, thus, follows that we can indeed learn a lot by observing nature around us more closely to assist us with creating new interesting materials that mimic nature, rather than claiming to have found new morphologies.

1.7. References

[1] (a) P.J. Flory, *J. Chem. Phys.* **1942**, *10*, 51-61. (b) M.L. Huggins, *J. Phys. Chem.* **1942**, 151-158.

[2] (a) R.A. Jones and R.W. Richards, *Polymers at surfaces and interfaces*, pages 127-136. Cambridge university press, 1999. (b) F.S. Bates, *Science* **1991**, *251*, 898-905.

[3] E. Helfand and Z.R. Wasserman, Micro domain structures and the interface in block copolymers. In, *Developments in block copolymers,* I. Goodman Ed. volume 1, pages 99-125. Applied Science, London, 1982.

[4] A.K. Khandpur, S. Förster, F.S. Bates, I.W. Hamley, A.J. Ryan, W. Bras, K. Almdal, and K. Mortensen, *Macromolecules* **1995**, *28*, 8796-8806.

[5] (a) F.S. Bates and G.H. Fredickson, *Physics Today* **1999**, 32-38. (b) C.A. Tyler, J. Qin, F.S. Bates, and D.C. Morse, *Macromolecules* **2007**, *40*, 4654-4668. (c) T.H. Epps, E.W. Cochran, T.S. Bailey, R.S. Waletzko, C.M. Hardy, and F.S. Bates, *Macromolecules* **2004**, *37*, 8325-8341.

[6] M. Xenidou, F.L. Beyer, N. Hadjichristidis, S.P. Gido, and N. Beck Tan, *Macromolecules* **1998**, *31*, 7659-7667.

[7] Y. Matsushita, *Macromolecules* **2007**, *40*, 771-776.

[8] A.N. Semenov, *Macromolecules* **1993**, *26*, 6617-6621.

[9] L. Leibler, *Macromolecules* **1980**, *13*, 1602-1617.

[10] M.W. Matsen and M. Schick, *Phys. Rev. Lett.* **1994**, *72*, 2660-2663.

[11] M.W. Matsen and F.S. Bates, *Macromolecules* **1996**, *29,* 1091-1098.

[12] A. Ciferri, *Supramolecular Polymers*, 2nd ed.; CRC Press, 2005.

[13] M.W. Matsen and M. Schick, *Macromolecules* **1994**, *27*, 6761-6767.

[14] M.W. Matsen, *J. Phys. Condens. Matter* **2002**, *14*, R21-R47.

[15] (a) S. O'Driscoll, G. Demirel, R.A. Farrell, T.G. Fitzgerald, C. O'Mahony, J.D. Holmes, and M.A. Morris, *Polym. Adv. Technol.* **2011**, *22*, 915-923. (b) H.-Y. Si, J.-S. Chen, and G.-M. Chow, *Colloids and Surfaces A: Physicochem. Eng. Aspects* **2011**, *373*, 82-87.

[16] P. Escalé, L. Rubatat, C. Derail, M. Save, L. Billon, *Macromol. Rapid Commun.* **2011**, *32*, 1072-1076.

[17] (a) X. Zhang, Y. Qiao, L. Xu, and J.M. Buriak, *ACS Nano* **2011**, *5*, 5015-5024. (b) Q. Lou, P.S. Chinthamanipeta, and D.A. Shipp, *Langmuir* **2011**, *27*, 15206-15212. (c) Y. Zhang, Q. Wang, *Macromol. Rapid Commun.* **2011**, *32*, 1645-1651. (d) S.P. Nunes, M. Karunakaran, N. Pradeep, A.R. Behzad, B. Hooghan, R. Sougrat, H. He, and K.-V. Peinemann, *Langmuir* **2011**, *27*, 10184-10190.

[18] K.-V. Peinemann, V. Abetz, and P.F.W. Simon, *Nature Materials* **2007**, *6*, 992-996.

[19] S. Park, B. Kim, O. Yavuzcetin, M.T. Tuominen, and T.P. Russell, *ACS Nano* **2008**, *2*, 1363-1370.

[20] P.S. Jo, Y.J. Park, S.J. Kang, T.H. Kim, C. Park, E. Kim, D.Y. Ryu, and H.-C. Kim, *Macromol. Res.* **2010**, *18*, 777-786.

[21] X. Zu, J. Gong, W. Tu, and Y. Deng, *Macromol. Rapid Commun.* **2011**, *32*, 1526-1532.

[22] J. Hong, J. Cho, K. Char, Journal of Colloid and Interface Science **2011**, *364*, 112-117.

[23] J.-M. Lehn *Science* **1993**, *260*, 1762-1763.

[24] (a) O. Ikkala, J. Ruokolainen, G. ten Brinke, M. Torkkeli, and R. Serimaa, *Macromolecules* **1995**, *28*, 7088-7094. (b) J. Ruokolainen, R. Mäkinen, M. Torkkeli, T. Mäkelä, R. Serimaa, G. ten Brinke, and O. Ikkala, *Science* **1998**, *280*, 557-560. (c) J. de Wit, G.O.R. Alberda van Ekenstein, E. Polushkin, K. Kvashnina, W. Bras, O. Ikkala, and G. ten Brinke, *Macromolecules* **2008**, *41*, 4200-4204.

[25] J. Ruokolainen, G. ten Brinke, O. Ikkala, M. Torkkeli, and R. Serimaa, *Macromolecules* **1996**, *29*, 3409-3415.

[26] J. Ruokolainen, G. ten Brinke, and O. Ikkala, *Adv. Mater.* **1999**, *11*, 777-780.

[27] J. Ruokolainen, M. Saariaho, O. Ikkala, G. ten Brinke, E.L. Thomas, M. Torkkeli, and R. Serimaa, *Macromolecules* **1999**, *32*, 1152-1158.

[28] J. Ruokolainen, M. Torkkeli, R. Serimaa, B.E. Komanschek, O. Ikkala, and G. ten Brinke, *Phys. Rev. E* **1996**, *54*, 6646-6649.

[29] S. Valkama, T. Ruotsalainen, A. Nykänen, A. Laiho, H. Kosonen, G. ten Brinke, O. Ikkala, and J. Ruokolainen, *Macromolecules* **2006**, *39*, 9327-9336.

[30] G.O.R. Alberda van Ekenstein, R. Meyboom, and G. ten Brinke, *Macromolecules* **2000**, *33*, 3752-3756.

[31] E. Polushkin, G.O.R. Alberda van Ekenstein, M. Knaapila, J. Ruokolainen, M. Torkkeli, R. Serimaa, W. Bras, I. Dolbnya, O. Ikkala, and G. ten Brinke, *Macromolecules* **2001**, *34*, 4917-4922.

[32] (a) W. van Zoelen, T. Asumaa, J. Ruokolainen, O. Ikkala, and G. ten Brinke, *Macromolecules* **2008**, *41*, 3199-3208. (b) W. van Zoelen, E. Polushkin, and G. ten Brinke, *Macromolecules* **2008**, *41*, 8807-8814.

[33] (a) G. Gobius du Sart, I. Vukovic, Z. Vukovic, E. Polushkin, P. Hiekkataipala, J. Ruokolainen, K. Loos, and G. ten Brinke, *Macromol. Rapid Commun.* **2010**, *32*, 366-370. (b) G. Gobius du Sart, I. Vukovic, G.O.R. Alberda van Ekenstein, E. Polushkin, K. Loos, and G. ten Brinke, *Macromolecules* **2010**, *43*, 2970-2980.

[34] G. ten Brinke, K. Loos, I. Vukovic, and G. Gobius du Sart, *J. Phys.: Condens. Matter* **2011**, *23*, 1-6.

[35] C.-H. Lee and S.-H. Tung, *Soft Matter* **2011**, *7*, 5660-5668.

[36] J.T. Korhonen, T. Verho, P. Rannou, and O. Ikkala, *Macromolecules* **2010**, *43*, 1507-1514.

[37] B.K. Kuila, E.B. Gowd, and M. Stamm, *Macromolecules* **2010**, *43*, 7713-7721.

[38] C. Wang, T. Wang, Q. Wang, *Polymer* **2010**, *51*, 4836-4842.

[39] A.J. Meuler, M.A. Hillmyer, and F.S. Bates, *Macromolecules* **2009**, *42*, 7221-7250.

[40] L.E. Scriven, *Nature* **1976**, *263*, 123-125.

[41] D.B. Alward, D.J. Kinning, E.L. Thomas, L.J. Fetters, *Macromolecules* **1986**, *19*, 215-224.

[42] A.H. Schoen, NASA TN D-5541, **1970**.

[43] T. Hashimoto, Y. Nishikawa, and K. Tsutsumi, *Macromolecules* **2007**, *40*, 1066-1072.

[44] (a) H.-Y. Hsueh, H.-Y. Chen, M.-S. She, C.-K. Chen, R.-M. Ho, S. Gwo, H. Hasegawa, and E.L. Thomas, *Nano Lett.* **2010**, *10*, 4994–5000. (b) V.N. Urade, T.-C. Wei, M.P. Tate, J.D. Kowalski, and H.W. Hillhouse, *Chem. Mater.* **2007**, *19*, 768-777. (c) A.M. Urbas, M. Maldovan, P. DeRege, and E.L. Thomas, *Adv. Mater.* **2002**, *14*, 1850-1853. (d) V.Z.-H. Chan, J. Hoffman, V.Y. Lee, H. Latrou, A. Avgeropoulos, N. Hadichristidis, R.D. Miller, and E.L. Thomas, *Science* **1999**, *286*, 1716-1719.

[45] E.W. Cochran, C.J. Garcia-Cervera, and G.H. Fredrickson, *Macromolecules* **2006**, *39*, 2449-2451.

[46] I. Vukovic, S. Punzhin, Z. Vukovic, P. Onck, J.T.M. De Hosson, G. ten Brinke, and K. Loos, *ACS Nano* **2011**, *5*, 6339-6348.

[47] I. Ohno, *Materials Science and Engineering* **1991**, *A146*, 33-49.

[48] A. Brenner and G. Ridell, *J. Res. Natl. Bur. Stand.* **1946**, *37*, 1725.

[49] A. Wurtz, *C. R. Acad. Sci.* **1844**, *18*, 702.

[50] (a) K.H. Krishnan, S. John, K.N. Srinivasan, J. Praveen, M. Ganesan, and P.M. Kavimani, *Metallurgical and Materials Transactions A* **2006**, *37A*, 1917-1926. (b) B.D. Barker, *Surface Technology* **1981**, *12*, 77-88. (c) J.N. Balaraju, T.S.N. Sankara Narayanan, and S.K. Seshadri, *Journal of Applied Electrochemistry* **2003**, *33*, 807-816.

[51] T. Hashimoto, K. Tsutsumi, and Y. Funaki, *Langmuir* **1997**, *13*, 6869-6872.

[52] H.-Y. Hsueh, Y.-C. Huang, R.-M. Ho, C.-H. Lai, T. Makida, and H. Hasegawa, *Adv. Mater.* **2011**, 1-6.

[53] (a) E.J.W. Crossland, M. Kamperman, M. Nedelcu, C. Ducati, U. Wiesner, D.-M. Smilgies, G.E.S. Toombes, M.A. Hillmyer, S. Ludwigs, U. Steiner, and H.J. Snaith, *Nano Letters* **2009**, *9*, 2807-2812. (b) E.J.W. Crossland, S. Ludwigs, M.A. Hillmyer, and U. Steiner, *Soft Matter* **2010**, *6*, 670-676.

[54] Y. Okinaka, Chapter 15 Electroless Plating of Gold and Gold Alloys. In, *Electroless Plating: Fundamentals And Applications,* G.O. Mallory and J.B. Hajdu, Ed. Reprint Edition, pages 414-420. American Electroplaters and Surface Finishers Society, Orlando, Florida, 1990.

[55] I. Ohno, Chapter 22 Electroless Deposition of Alloys. In, *Modern Electroplating, Fifth Edition*, M. Schlesinger and M. Paunovic, Ed. Pages 499-506.John Wiley & Sons, Inc., 2010.

[56] V. Saranathan, C.O. Osuji,, S.G.J. Mochrie, H. Noh, S. Narayanan, A. Sandy, E.R. Dufresne, and R.O. Prum, *PNAS* **2010**, *107*, 11676-11681.

2. Results and discussion

2.1. The phase diagram of PS-b-P4VP(PDP)$_x$

For the investigation of the phase behavior of the supramolecular complex PS-*b*-P4VP(PDP)$_x$ we studied a series of BCPs which we arranged in three groups: the first group (i) had a ratio, *r*, between the PS and P4VP block-length of $r \approx 2.5$, the second group (ii) with $r < 2.5$, and the third group (iii) with $r > 2.5$. We varied the amount of added PDP and the molar mass of the block copolymer precursor to investigate for which conditions the bicontinuous gyroid morphology is obtained. We used Microtoming[1] to fabricate thin sections of the PS-*b*-P4VP(PDP)$_x$ films and investigated the bulk microphase separated morphologies with TEM[2] and SAXS.[3]

If we assume equal densities for all components, we can express the volume fraction of the comb block, i.e., the volume fraction of P4VP complexed with PDP, as follows:

$$f\big(P4VP(PDP)\big) = \frac{M(PDP)+M(P4VP)}{M(PDP)+M(P4VP)+M(PS)} \quad (1).$$

The volume fraction is expressed as *f* and *M* denotes mass. The mass of PDP can be expressed by the number of units, *N(PDP)*, multiplied by its molar mass and, because the amount of PDP is related to the number of P4VP monomer units, *N(P4VP)*, via *x*, we write that:

$$M(PDP) = N(PDP) \cdot 304\ g/mol\ = N(P4VP) \cdot x \cdot 304\ g/mol \quad (2)$$

and

$$M(PDP) = \frac{M(P4VP)}{105\ g/mol} \cdot x \cdot 304\ g/mol\ \approx 3x \cdot M(P4VP) \quad (3).$$

Here, *x*, denotes the number of PDP molecules relative to the number of 4VP units. By substituting equation 3 in equation 1 we find that:

$$f\big(P4VP(PDP)\big) \approx \frac{3x \cdot M(P4VP)+M(P4VP)}{3x \cdot M(P4VP)+M(P4VP)+M(PS)} \approx \frac{3x+1}{3x+1+M(PS)/M(P4VP)} \quad (4)$$

and finally

$$f\big(P4VP(PDP)\big) \approx \frac{3x+1}{3x+1+r} \quad (6).$$

In this equation for the volume fraction of the comb block, the ratio between the mass of PS and P4VP is written as $r = (M(PS))/(M(P4VP))$. In previous experiments the gyroid morphology was found at a

volume fraction of 0.62. If we use this value of *f* in our calculations we can estimate for which value of *x* the gyroid morphology is to be expected for a BCP with a given ratio *r*. For group I we expect to find the gyroid morphology for $x = 1.0$, for group II at $x < 1.0$, and for group III at $x > 1.0$.

2.1.1. *Sample preparation method*

To all BCPs (with varying ratio *r*) we added a range of different concentrations of PDP (i.e., given by the value of *x*) and dissolved and homogenized these mixtures in chloroform for 24h. Next, we poured the solutions in Petri dishes and closed them with a lid. We then placed these Petri dishes in a larger container along with several open flasks containing fresh chloroform—which we refilled when necessary—to maintain a saturated chloroform vapor atmosphere, for slow solvent annealing. After complete evaporation of the solvent in the Petri dishes, we removed the samples and placed them in a vacuum oven at 30 ˚C for 24h to remove any residual solvent. We then put the Petri dishes in a sealable reactor chamber, evacuated the air, and then backfilled it with dry nitrogen, at an overpressure of 1.5 bar to minimize the leaching of PDP out of the complex at elevated temperatures. For temperature annealing of the samples we then placed the complete setup in an oven at 120 ˚C for 4 days.

After temperature annealing we cut the prepared films in smaller pieces with a razor blade and embedded these in epoxy in order to enable Microtome cutting of thin cross-sections of 80 nm thickness with a diamond knife. After cutting we transferred the thin sections from the water bath (i.e., attached to the knife) to a copper grid for analysis of the bulk morphology by TEM. Next, we stained the samples with iodine—to selectively stain P4VP to appear dark—for 45 minutes, followed by visually determining the morphology of the films. By looking at multiple sections and positions, we checked whether the morphology is the same throughout the film. Of all the prepared samples we also collected SAXS data in order to validate if the observed morphologies by TEM are macroscopic by calculating the peak position ratios. A complete list of the samples that we prepared in this master's thesis is given in Table 3 and the results of the TEM measurements, along with the results that were obtained earlier in our group, are summarized in Graph 1, Graph 2, and Graph 3 for group I, II and III, respectively.

Table 3. *A complete overview of the prepared samples from each group and the morphology as determined by TEM.*

Exp. ID	PDI	M (PS)	M (P4VP)	M_{total} [a]	N (BCP)	x	r (PS/P4VP)	f (P4VP(PDP)$_x$)	Group	Morphology [b]
IV041	1.30	37,500	16,000	100,000	535	1.00	2.3438	0.6243	I	CYL
IV042	1.30	37,500	16,000	95,000	535	0.90	2.3438	0.6061	I	GYR + CYL
IV043	1.10	24,000	9,500	61,000	335	1.00	2.5263	0.6066	I	GYR
IV045	1.30	37,500	16,000	91,000	535	0.80	2.3438	0.5859	I	GYR
IV061	1.10	24,000	9,500	58,000	335	0.90	2.5263	0.5880	I	GYR
IV092	1.09	12,000	9,500	31,000	215	0.35	1.2632	0.6145	II	LAM
IV093	1.09	12,000	9,500	34,000	215	0.45	1.2632	0.6458	II	CYL
IV094	1.15	27,000	16,500	69,000	435	0.53	1.6364	0.6077	II	LAM
IV095	1.15	27,000	16,500	71,000	435	0.57	1.6364	0.6183	II	GYR + CYL
IV096	1.09	35,000	21,000	88,000	560	0.53	1.6667	0.6033	II	LAM + GYR
IV097	1.09	35,000	21,000	91,000	560	0.57	1.6667	0.6139	II	GYR
IV098	1.09	41,000	24,000	96,000	650	0.45	1.7083	0.5741	II	LAM
IV099	1.09	41,000	24,000	100,000	650	0.50	1.7083	0.5889	II	LAM
IV100	1.09	41,000	24,000	100,000	650	0.55	1.7083	0.6028	II	LAM + GYR
IV101	1.09	41,000	24,000	110,000	650	0.65	1.7083	0.6278	II	GYR + CYL
IV102	1.09	41,000	24,000	120,000	650	0.75	1.7083	0.6499	II	GYR
IV103	1.10	25,000	7,000	64,000	320	1.60	3.5714	0.6120	III	GYR + CYL
IV104	1.10	25,000	7,000	68,000	320	1.80	3.5714	0.6349	III	GYR + CYL
IV105	1.15	50,000	17,000	125,000	670	1.17	2.9412	0.5987	III	CYL
IV106	1.15	50,000	17,000	128,000	670	1.24	2.9412	0.6095	III	CYL

[a] *Values are rounded up.* [b] *According to TEM results.*

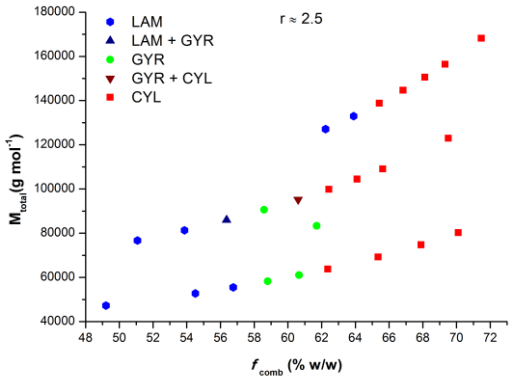

Graph 1. *The phase diagram of group I with r ≈ 2.5 shows that at the lower part of the phase diagram PS-b-P4VP(PDP)$_x$ transitions from lamellae to the gyroid morphology and finally cylinders are present. The single point at a volume fraction of 0.62 and a total mass of 80,000 is the first sample where the gyroid morphology was found experimentally, however, there was not enough material left to complete this part of the phase diagram. At higher total molecular weights we find that with increasing number of monomer units of the block copolymer precursor, the gyroid morphology region decreases in size. Furthermore, biphasic morphologies are observed that consist of lamellae combined with the gyroid morphology or a gyroid morphology combined with cylinders. In the upper part we find no gyroid morphology.*

2.1.2. *Morphological study by transmission electron microscopy*

In the introduction we discussed that it was previously found that the addition of the PDP to PS-*b*-P4VP(PDP)$_x$ lowers the Flory-Huggins interaction parameter (i.e., the χ-parameter), causing the system to be in the intermediate segregation regime, rather than the strong segregation regime as is the case with the pure BCP. The χ-parameter of the pure BCP is known to be around 0.34, however, because the value of the interaction parameter between the blocks is lowered by PDP we were unable to construct a classical phase diagram. Therefore, we plotted the total molar mass of the supramolecular complex against the volume fraction of the comb block. Each "line" of data points represents one BCP composition that increases in total molar mass because of an increasing concentration of PDP (i.e., an increasing f_{comb}).

In the phase diagram of group I (Graph 1) we observe that at the lower part of the phase diagram PS-*b*-P4VP(PDP)$_x$ transitions from lamellae to the gyroid morphology and finally cylinders are present. Furthermore, we note that the width of the gyroid region in the phase diagram becomes more narrow with increasing molar mass of the BCP precursor, which is in accordance with SCFT calculations.[4] The single point at a volume fraction of 0.62 and a total mass of 80,000 is the first sample where the gyroid morphology was found experimentally, however, there was not enough BCP left to complete this part of the phase diagram. In this master's thesis we will try to synthesize this polymer via anionic polymerization (see section 2.3). At a somewhat higher mass in the phase diagram, besides the expected transition (i.e., LAM→GYR→CYL) we also find films that have two coexisting morphologies. The first biphasic morphology is positioned between the lamellar and gyroid morphology, at low volume fractions, and consists of lamellar and gyroid grains. The second biphasic morphology we observe at higher volume fractions where the gyroid morphology exists along with cylindrical grains, at a position between the gyroid and cylindrical morphology. In particular, the size of the individual grains of this biphasic morphology can be large, i.e., some parts of the films consist solely of the gyroid morphology and other parts only of a cylindrical morphology. There are indications that a biphasic morphology can been attributed to a polydispersity effect in mixtures of BCPs with equal *N* but different PDIs of one of the blocks.[5] However, in our case it is most likely caused by the nature of the supramolecular complex and does not come as a surprise. Biphasic

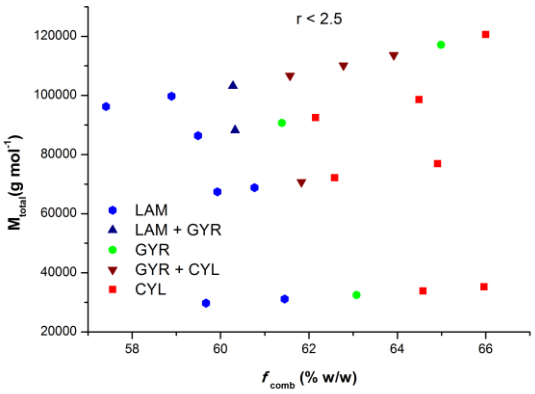

Graph 2. *The phase diagram of group II with r < 2.5 shows that at the lower part of the phase diagram the BCP complex behaves similarly as a regular BCP (i.e., LAM → GYR → CYL) and in the middle of the phase diagram a biphasic morphology with gyroid and cylinders is observed in between lamellae and cylinders. At the upper part of the phase diagram we observe a wide region of a biphasic morphology.*

morphologies have been observed before in homopolymer/block copolymer blends and they appear most likely due to the gradient of homopolymer concentration in the sample. Because PDP can locate itself near the boundaries between the different blocks of PS-*b*-P4VP, a diffuse interface is obtained, which might allow the biphasic morphologies that we observe. It is very common that a two component mixture (i.e., PDP and PS-*b*-P4VP) macrophase separates, in our case, however, this macrophase separation results in the formation of two phases with different microphase separated structures. Furthermore, a high polydispersity usually results in broader interfaces and higher long periods.[6] When *N* becomes too large the segregation between the individual blocks becomes stronger and the gyroid morphology is no longer observed, instead a lamellar morphology immediately changes to the cylindrical morphology. In summary, the double gyroid network morphology can be found for $0.58 < f_{comb} < 0.62$ (by changing the concentration of PDP as $0.8 < x < 1.0$) of a BCP with a total degree of polymerization of $335 < N < 535$ with $r \approx 2.5$ (i.e., group I).

At low molecular weight the supramolecular complexes from group II (Graph 2) behave in the same way as the complexes from group I at the lower part of the phase diagram; first lamellae, then the gyroid morphology, and finally cylinders appear. The window of volume fractions where we find the gyroid morphology is very small, in particular the supramolecular complex obtained from PS(12,000)-*b*-P4VP(9,500) has a gyroid morphology for $x = 0.40$ but gives a lamellar morphology at $x =$

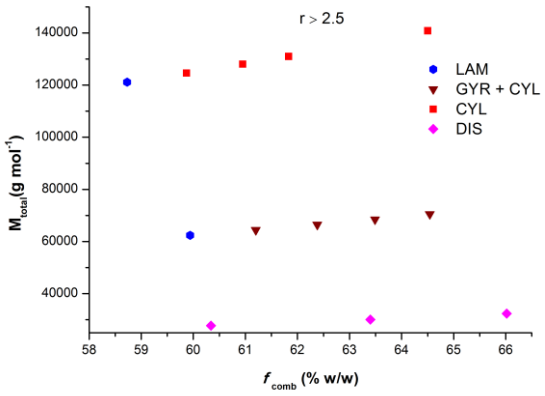

Graph 3. *The phase diagram of group III with r > 2.5 shows that at low values of the total molar mass the length of the P4VP(PDP)$_x$ becomes too short to induce microphase separation because the system is below the weak segregation limit and becomes disordered. At high values of the total molar mass we observe a direct transition of lamellae into cylinders. Furthermore, we do not observe the gyroid morphology as a pure phase in this group.*

0.35 and a cylindrical morphology for x = 0.45. With increasing N we often find biphasic morphologies in the complexes but also pure gyroid. At a higher molecular weight of about 90,000 we observe the gyroid morphology positioned at the right side of a biphasic morphology of lamellae with gyroid and the next morphology we find is cylinders. We observe a similar pattern with films generated from a BCP with an even higher molecular weight where we first find lamellae, then a biphasic morphology of lamellae and gyroid, next a biphasic morphology of gyroid and cylinders, followed by the gyroid morphology, and finally cylinders again. This demonstrates the complex behavior of the supramolecular complex of PS-*b*-P4VP(PDP)$_x$ in which adding PDP not only increases the volume fraction of the P4VP block, but also influences the effective interaction parameter of both blocks. Furthermore, we observe that the films from group II consisted of smaller grains compared to those prepared from group I. In summary, in group II the double gyroid morphology can be found for 0.61 < f_{comb} < 0.65 (by changing the concentration of PDP as 0.4 < x < 0.8) of a BCP with a total degree of polymerization of 215 < N < 650 with r < 2.5.

The phase diagram of group III (Graph 3) shows that at low molecular weights we observe disordered microphase separated films because the total number of units (N) of the starting BCP are too low. In the case of pure BCP $\chi N \sim 50$ for this sample which would mean that the system is in the strong segregation regime. Therefore, the observed disordered microphase separated morphologies

are again proof that PDP lowers the interaction parameter. The BCP complex is below the weak segregation threshold and, therefore, cannot microphase separate in ordered domains. At high molecular weights a lamellar morphology immediately passes into a cylindrical morphology which is consistent with observations from group I. At a total molecular weight of about 60,000 we first find lamellae and then a broad biphasic region of gyroid and cylinders. Because we do not find the gyroid morphology in group III (as a single morphology), this group is not very useful when considering a gyroid porous polymer template. It has been shown in our group, however, that a metal nanofoam could be generated from a BCP complex with a cylindrical morphology. After removal of the polymer by pyrolysis one would expect the metal to collapse since the supporting matrix is removed. However, by TEM analysis it has been shown that this is not the case due to imperfections in the morphology and because the film consists out of different grains, thereby, the metal did not collapse. Thus, it follows that the biphasic morphology of gyroid with cylinders can also be used to generate, albeit a less perfect, metal nanofoam. In summary, the gyroid morphology is only present as a biphasic morphology for $0.61 < f_{comb} < 0.65$ (by changing the concentration of PDP as $1.6 < x < 1.9$) of a BCP with a total degree of polymerization of $N = 320$ with $r > 2.5$.

2.1.3. *Morphological study by small angle x-ray scattering*

Above results and discussions we based on TEM measurements only and of all the samples that we prepared in this master's thesis we also collected SAXS data at the University of Helsinki. SAXS is a powerful tool to use in morphological studies because the scattering patterns obtained from a film are macroscopic, whilst TEM images represent only a small portion of the film. Different lattice types generate different reflection patterns with different specific allowed reflection peaks. A lamellar morphology has a scattering vector (q) of $q_h = h \cdot q^*$, for a hexagonally packed cylindrical morphology $q_{hk} = \sqrt{h^2 + hk + k^2} \cdot q^*$, and a body-centered cubic morphology (such as the gyroid morphology) is described by a scattering vector of $q_{hkl} = \sqrt{h^2 + k^2 + l^2} \cdot q^*$. Thus, by means of these equations, in which q^* is the first order reflection and *h, k, l = 0, 1, 2, 3, …,* we can determine the morphology of a film by calculating the peak positions relative to q^*.[7] The results of the SAXS measurements of the films from group I are summarized in Graph 4 (except for IV043), the SAXS data from group II are

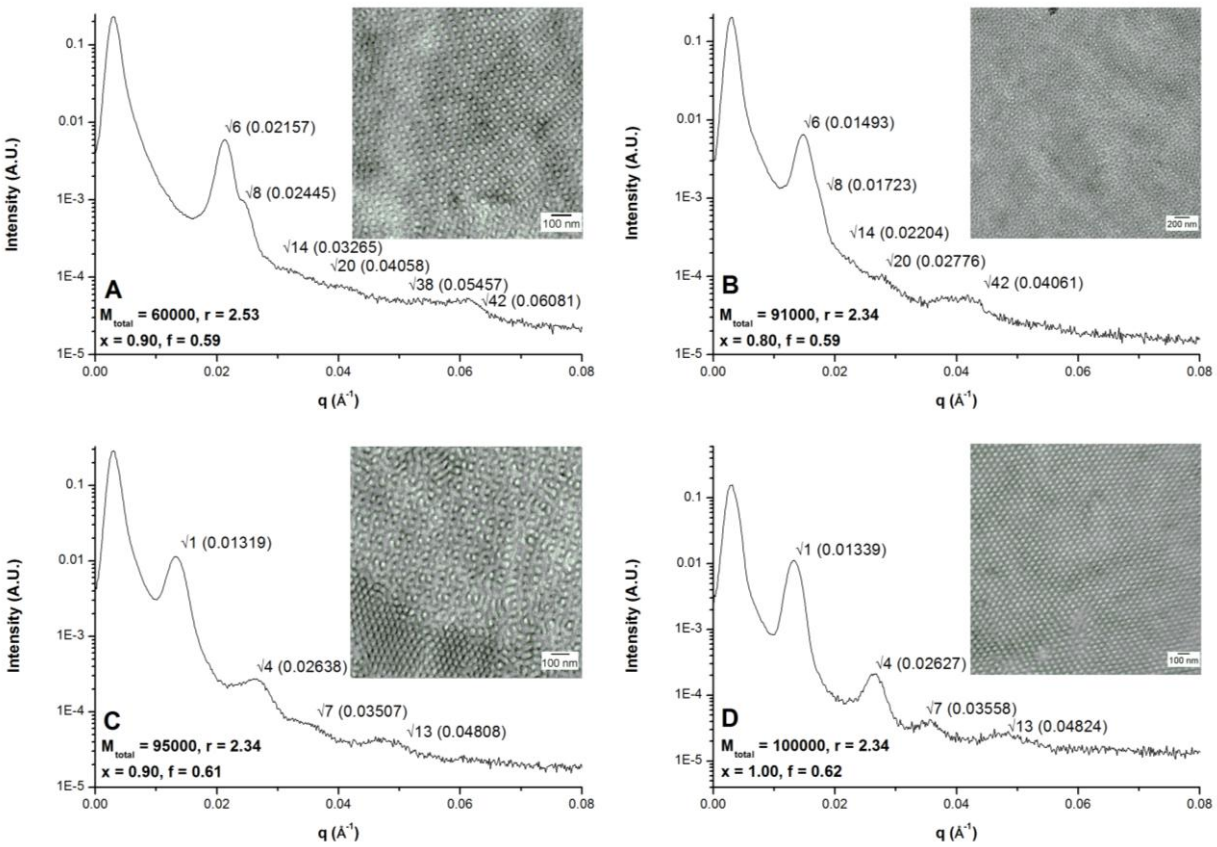

Graph 4. *Small angle X-ray scattering results from Helsinki measured with a 2.5 m long tube of samples from group I and in the inset the TEM results of the same film are shown with (A) the scattering pattern with the characteristic peaks belonging to a gyroid morphology; √6, √8, and higher scattering peaks. (B) The peaks of the scattering pattern belonging to a gyroid morphology are shifted to lower values of q because of a larger size of the unit cell. (C) The TEM image and the SAXS scattering pattern match the characteristic pattern for a cylindrical morphology. A √7 peak that is only visible for cylindrical morphologies is present. (D) The scattering pattern clearly shows the √7 peak indicating a cylindrical morphology which matches the TEM result.*

summarized in Graph 5 & Graph 6, and the SAXS results from group III are summarized in Graph 7. The first peak that is present in all the SAXS patterns is from the beam stop that is used in the experimental setup (to prevent damage to the detector) and should not be considered as a diffraction peak from the sample.

The sample with M_{total} = 60,000 and f = 0.59 (Graph 4A) gives a SAXS scattering pattern with a peak that corresponds to √6 and a shoulder corresponding to √8. These two peaks form the key signature of a gyroid morphology that matches the TEM result. The next sample (Graph 4B) has a higher molecular weight, but the same volume fraction of the comb block, which also shows the signature peak corresponding to √6 and a shoulder corresponding to √8. This shoulder is less

pronounced compared to the previous sample mainly because the size of the unit cell is higher, due to a higher molecular weight of the BCP. Because of this, the first scattering peak is positioned closer to the beam stop peak where the sensitivity of the detector is lower and, therefore, the shoulder of √8 is less clearly visible.[8] The SAXS result of this sample, thus, matches the TEM result also. The sample with M_{total} = 95,000 and f = 0.61 (Graph 4C) has a SAXS scattering pattern with a peak corresponding to √7, which is only visible for a hexagonally ordered cylindrical morphology, however, the TEM result (inset) shows a biphasic morphology of gyroid with cylinders. It is possible that the gyroid grains are small or have poor ordering and, therefore, are not visible in the SAXS pattern. The sample with a somewhat higher molecular weight of 100,000 and a volume fraction of 0.62 shows the characteristic peak corresponding to √7 and, hence, the cylindrical morphology that is observed with TEM is confirmed. Based on the scattering peaks we can calculate the size of the unit cell of the gyroid morphologies.[9] The first peak of the sample with M_{total} = 60,000 is positioned at 0.216 nm which results in an interplanar spacing d ($d = 2\pi/q$) of 29 nm and a lattice parameter a ($a = \sqrt{6} \cdot d$) of 71 nm. Similarly, we find that for the sample with M_{total} = 91,000 the spacing d = 42 nm and the size of the unit cell a = 103 nm.

The SAXS data from the samples of group II up to a total molecular weight of 88,000 (Graph 5) are, unfortunately, inconclusive. Some peaks are visible but intensities are very small and in many cases the first scattering peak is missing or too close to the beam stop to be visible. The sample with M_{total} = 31,000 and f = 0.61 (Graph 5A) shows a lamellar morphology with TEM analysis, however, the first scattering peak of the corresponding SAXS result is positioned far from the beam stop because the lamellae of this sample are thin. Based on the peak ratio of two we can state that the SAXS pattern is in line with the TEM result. The next sample, with a somewhat higher molecular weight of 34,000 and a volume fraction of the comb block of 0.65 (Graph 5B), has a cylindrical morphology as determined by TEM. Unfortunately, the first scattering peak is missing and there is only one peak visible. Therefore, we cannot confirm the TEM result with the SAXS data. The following sample (Graph 5C; not included in the phase diagram), with M_{total} = 49,000 and f = 0.76, again misses the first scattering peak, however, the two peaks that are visible have a relative peak ratio and position that can correspond to √4 and √13. These scattering peaks are only visible with a cylindrical morphology,

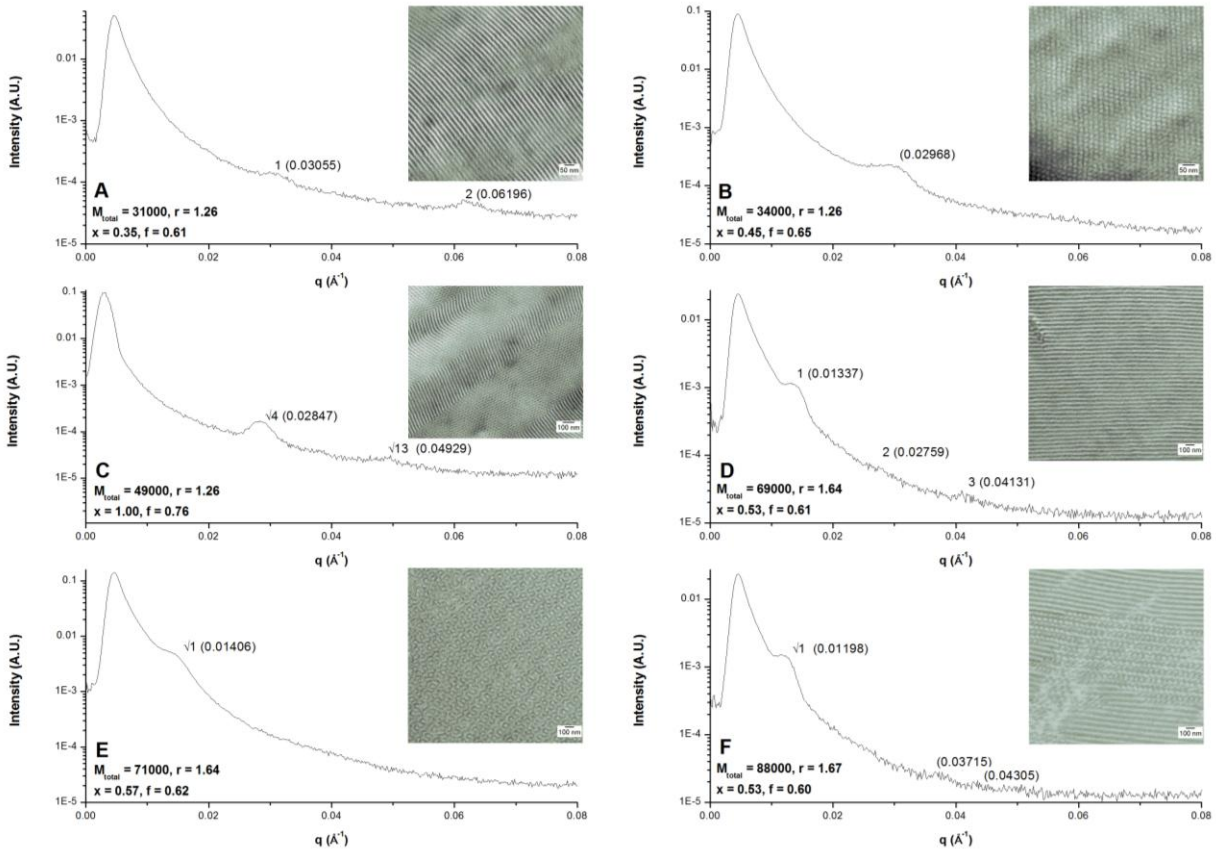

Graph 5. *Small angle X-ray scattering results from Helsinki measured with a 2.5 m long tube of samples from group II and in the inset the TEM results of the same film are shown with (A) M_{total} = 31,000 and f = 0.61, (B) M_{total} = 34,000 and f = 0.65, (C) M_{total} = 49,000 and f = 0.76, (D) M_{total} = 69,000 and f = 0.61, (E) M_{total} = 71,000 and f = 0.62, and (F) M_{total} = 88,000 and f = 0.60. The SAXS data of the samples from this group are inconclusive possibly because the films are not uniform in morphology and/or contain many (small) grains and orientations.*

thus, we can tentatively confirm the cylindrical morphology as determined by TEM. The next sample, with M_{total} = 69,000 and f = 0.61 (Graph 5D), has a first scattering peak that corresponds to q*, a small bump that is 2q*, and a third bump corresponding to 3q*. This scattering pattern is characteristic for a lamellar morphology and is in accordance with the TEM observation, however, intensities are very low. The film generated from a BCP complex with a total molar mass of 71,000, and a volume fraction of the comb of 0.61, is characterized as a biphasic morphology of the gyroid morphology with cylinders. The inset of Graph 5E shows a TEM image that consists of a gyroid morphology with several small and differently orientated grains, and other parts of the film consisted of poorly orientated cylinders (not shown). These observations made by TEM correspond to a poorly defined SAXS pattern with broad peaks and low intensities. The only shoulder that is visible for this sample can correspond

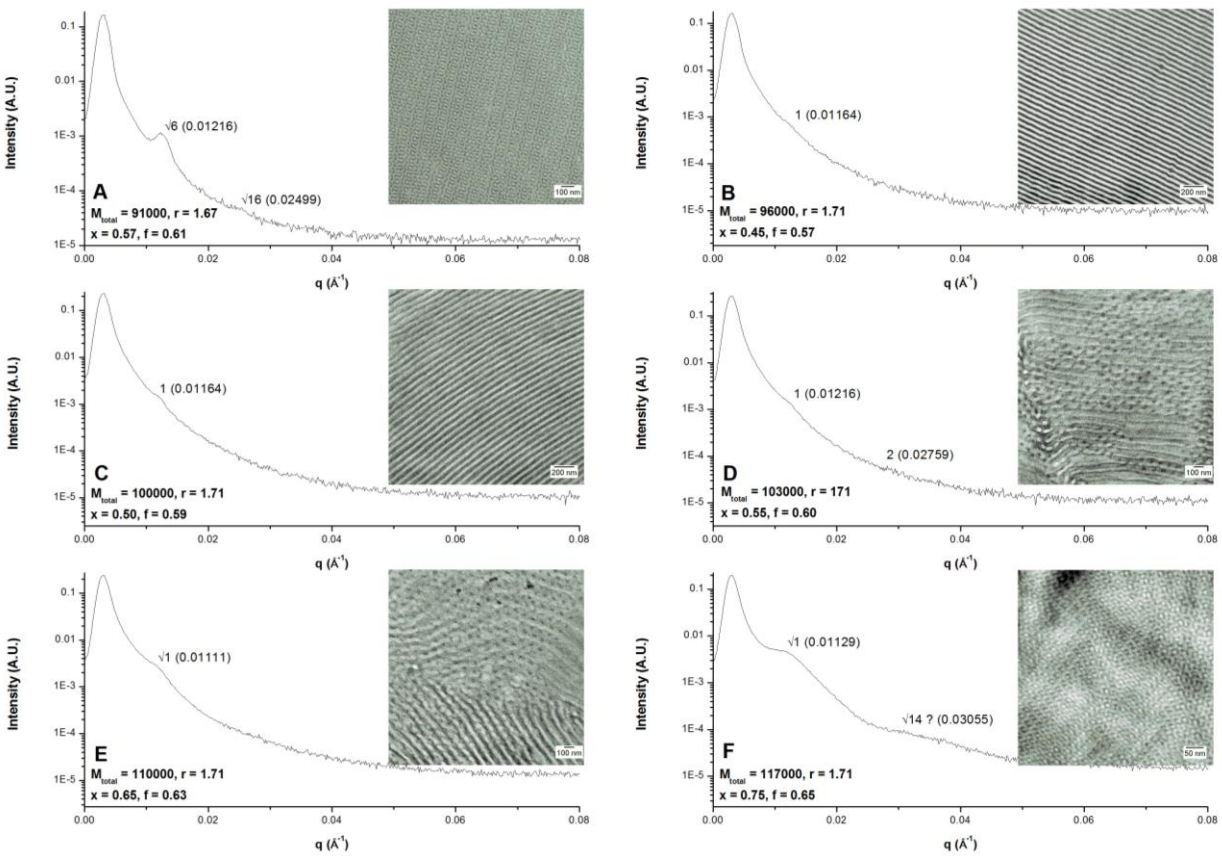

Graph 6. *Small angle X-ray scattering results from Helsinki measured with 2.5 m long tube and of samples from group II and in the inset the TEM results of the same film are shown with (A) M_{total} = 91,000 and f = 0.61, (B) M_{total} = 96,000 and f = 0.57, (C) M_{total} = 100,000 and f = 0.59, (D) M_{total} = 103,000 and f = 0.60, (E) M_{total} = 110,000 and f = 0.63, and (F) M_{total} = 117,000 and f = 0.65. The SAXS data of the samples from this group are also inconclusive possibly because the films are not uniform in morphology and/or contain many (small) grains and orientations.*

both to √1 for the cylindrical part or √6 for a gyroid with a large lattice parameter. The SAXS result for the next sample, with M_{total} = 88,000 and f = 0.60 (Graph 5F), is not much better than that of the previous one although there is some little more detail. The film has a biphasic morphology with a distorted gyroid morphology in between lamellar grains, as can be seen in the inset of Graph 5F. The intensities of the peaks in the resulting SAXS are very weak and there is allot of noise and, therefore, we cannot clarify the biphasic morphology further. The sample with M_{total} = 91,000 and f = 0.61 has a highly ordered gyroid morphology and its double wave projection is given in the inset of Graph 6A. Unfortunately, the SAXS pattern did not coincide with this TEM observation since the SAXS result has little detail. The first scattering peak can be assigned to √6 (indicating a = 127 nm), but the shoulder of √8 is missing, hence, the gyroid morphology, observed by TEM, cannot be confirmed by SAXS. It is

possible that the sample actually consist of many small and differently orientated grains, resulting in a poorly defined SAXS pattern. The next two samples, with a total molar mass of 96,000 and 100,000 (Graph 6B & C, respectively), show nearly no detail in the SAXS pattern and only one shoulder is barely visible, even though the TEM images show reasonably well ordered lamellae. Again it is possible that the films actually consists of many different grains and that the TEM images gives a skewed impression. The sample with M_{total} =103,000 and f = 0.60 (Graph 6D) shows a distorted biphasic morphology of lamellae with what seems to be a gyroid morphology, according to TEM. Unfortunately, the corresponding SAXS pattern does not give any more clarification of the morphology since there are only shoulders present which are barely visible. The resulting SAXS pattern of the next sample, with M_{total} = 110,000 and f = 0.63 (Graph 6E), also shows only one shoulder, thus, SAXS does not clarify the morphology further. The last sample from group II, with a total molecular weight of 117,000 and a volume fraction of the comb block of 0.65 (Graph 6F), shows two very broad shoulders that are difficult to identify. The TEM image, shown in the inset of Graph 6F, shows a gyroid morphology, however, the different grains are small and different plains are clearly distinguishable, resulting in a poorly defined SAXS pattern.

With the samples from group III we observe similar results with SAXS compared to group II; poorly defined scattering patterns and low peak intensities. The samples with a total molar mass of 64,000 and 68,000 (Graph 7A & B, respectively) both consist of a biphasic morphology of the gyroid morphology with cylinders. However, the SAXS patterns of both films contains only one broad “peak” positioned at approximately 0.02 Å, which can be carefully identified as √6, by simply comparing peak positions with previous results that contained the gyroid morphology. However, since other peaks are missing we cannot draw any conclusions. The next two samples, with M_{total} = 125,000 and M_{total} = 128,000 (Graph 7C & D, respectively), have a hexagonally packed cylindrical morphology according to TEM analysis. However, the SAXS data of both films lack any form of detail, probably because the macroscopic ordering is too poor.

2.1.4. *Tunable polymer template porosity*

Above, we discussed the phase behavior of PS-*b*-P4VP(PDP)$_x$ as we observed by TEM and

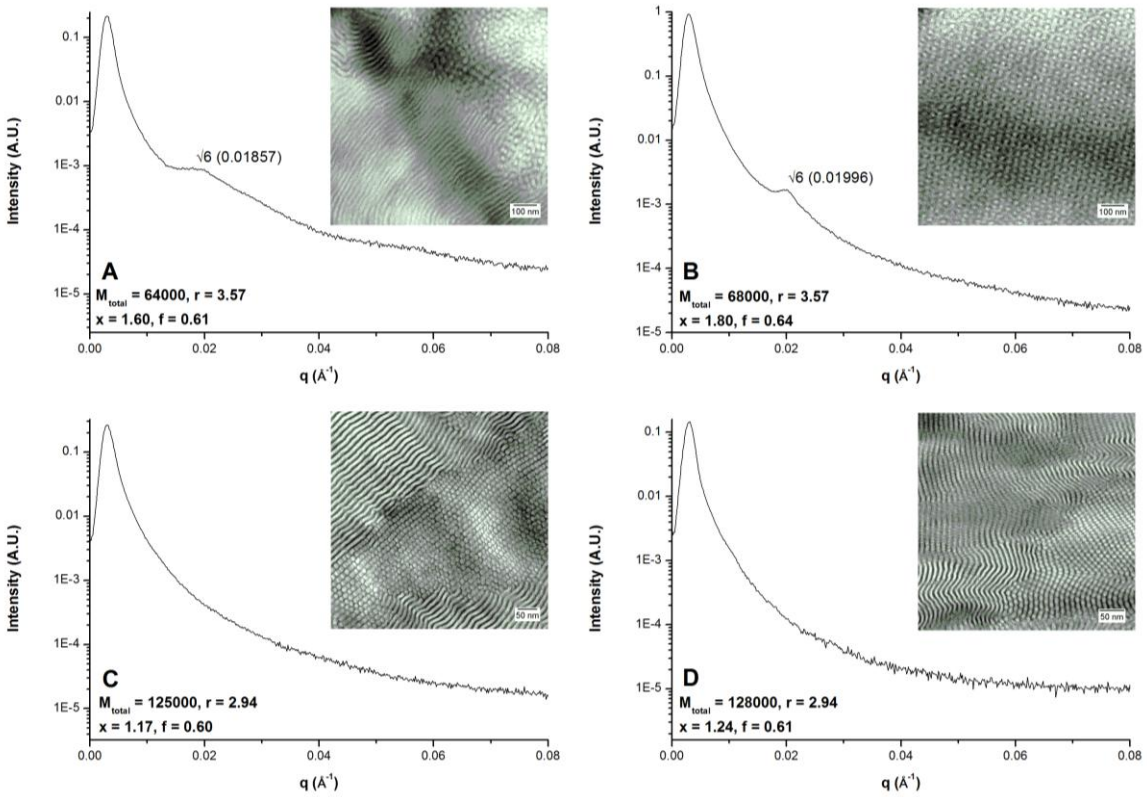

Graph 7. *Small angle X-ray scattering results from Helsinki measured with 2.5 m long tube of samples from group III and in the inset the TEM results of the same film are shown with (A) M_{total} = 64,000 and f = 0.61, (B) M_{total} = 68,000 and f = 0.64, (C) M_{total} = 125,000 and f = 0.60, and (D) M_{total} = 128,000 and f = 0.61. The SAXS data of the samples from this group are also inconclusive possibly because the films are not uniform in morphology and/or contain many (small) grains and orientations.*

SAXS analysis. The justification of the investigation for the complete phase behavior of PS-*b*-P4VP(PDP)$_x$, is that, by moving from group I to group II or group III, the porosity of the (double gyroid) films can be chosen. When PDP is selectively removed by soaking a film in ethanol the resulting porosity of the polymer template is dependent of the original volume fraction of the PDP in the complex. In group II we have to add less PDP to the system compared to group I, to reach the gyroid morphology at a volume fraction of $\sim$ 0,62 for the comb block and, thus, the porosity after PDP removal becomes less also. In the case of films from group III the situation is opposite compared to group II since we have to add more PDP to reach the gyroid morphology (according to our calculations), hence, the porosity of the polymer template after PDP removal is larger compared to group I. When the porous polymer template is backfilled with, e.g., nickel, the percentage of porosity of the metal nanofoam after pyrolysis is the inverse of the porosity percentage of the polymer

Table 4. *A comparison of the relative porosities of porous films generated from the three different groups. The concentration of PDP in group I ranges around x ≈ 1.0, to group II we add less PDP relative to group I (x ≈ 0.6), and we add more PDP to samples of group III. By adding more or less PDP a template with a higher or lower porosity, respectively, is obtained and, thereby, a metal nanofoam with a respectively lower or higher porosity.*

Group	Composition of PS(blue)-*b*-P4VP(red)	[PDP]	Template porosity	Metal foam porosity
I		=	=	=
II		<	<	>
III		>	≥	≤

template. Thus, the metal nanofoams obtained from a gyroid morphology from group I have a lower porosity than a metal nanofoam obtained from a gyroid morphology from group II, but lager than nanofoams from group III, as is summarized in Table 4. For example, we can calculate the porosities of a sample, with the gyroid morphology, from group I by expressing the concentration of PDP in the complex as follows: $3x \cdot M_{P4VP}/(3x + r \cdot M_{P4VP} + M_{P4VP})$. When *x* = 1.0 and *r* = 2.45 we find that the porosity of the template after PDP removal is 46.5% and, hence, the porosity of the metal nanofoam will be 53.5%. Similarly, if *x* = 0,5 and *r* = 1,7 the porosity of the template is 35.7% and the metal nanofoam 64.3%. With *x* = 1,5 and *r* = 3.0 we find a porosity of 52.9% and 47.1% for the polymer template and the metal nanofoam, respectively. By picking films with the gyroid morphology from the three different groups we are, thereby, capable of choosing the porosity of, for example, metal nanofoams.

2.2. The position of PDP in the complex

In earlier experiments it was discovered that although PDP favorably complexes to the 4VP units, it also migrates, to some extent, into PS.[10,11] In our procedure to generate the supramolecular complex films we calculated the concentration of PDP, that we needed to add to a PS-*b*-P4VP BCP, according to the weight of the P4VP block, expressed as *x*. For this calculation we assumed that PDP is only in the P4VP phase and, therefore, we are interested to know how much PDP actually goes to the PS phase. Plasticizers are known to influence the glass-transition temperature (T_g) of a polymer to a large extend[12], therefore we used differential scanning calorimetry[13] (DSC) to find the correlation between the PDP concentration and the T_g of PS. Unfortunately, DSC is not very suitable to

quantitatively determine the fraction of PDP that migrates into PS. We can, however, use DSC to qualitatively determine the effect of PDP on the T_g of PS and thereby deduce the position of PDP in the complex at various concentrations. We measured the T_gs of PS in PS-*b*-P4VP(PDP)$_x$ with varying values of *x* and also the T_gs of PS in PS homopolymer/PDP mixtures with varying weight percentages of PDP.

2.2.1. *The glass-transition temperature of PS in PS-b-P4VP mixed with PDP*

Earlier experiments done in our group showed that PDP lowers the T_g of P4VP by a huge value from 146 ˚C to approximately 25 ˚C, where it is overlapped by the melting peak of PDP. [14] Here, we only monitor the T_g of PS at different concentrations of PDP. In our first experiment we keep the BCP molecular weight constant and only vary the concentration of PDP in the system. For this experiment we used a BCP with a high molecular weight to improve the visibility of the different transitions. Some of the samples were prepared earlier (with $x > 0.70$) and some (with $x < 1.00$) we prepared via a solvent evaporation (without annealing); PS(48000)-*b*-P4VP(20300) with $x = 1.70$, x = 1.30, $x = 1.00$, $x = 0.70$, $x = 0.30$, and $x = 0.10$. The sample of pure BCP was used as received from Polymer Source and the results of this experiment are summarized in Graph 8. Large peaks are clearly visible in Graph 8A that belong to the melting temperature of PDP and, when the concentration of PDP drops below $x = 0.70$ these peaks are no longer observed. Also visible are order-disorder-transitions (ODTs) at moderate PDP concentrations, shown as small peaks in Graph 8B. The T_g of each trace belongs to PS which drops drastically from 107˚C for pure PS-*b*-P4VP ($x = 0.00$) to 70 ˚C for $x = 1.70$. These measurements appear to confirm that a fraction of PDP, even at very low concentrations, migrates into the PS phase, thereby lowering the T_g of PS. At low concentrations of PDP, and especially for the sample with no PDP, we should be able to assign a T_g to P4VP, however, with the scanning speeds that we used, the baseline contains a lot of noise in the temperature range where we would expect the T_g of P4VP and, therefore, we cannot assign a T_g. Luyten *et al.* suggested that at lower or equal to stoichiometric concentrations, PDP can form lamellar domains in between P4VP layers and crystallize in an interdigitating fashion. At higher than stoichiometric concentrations the lamellar domain spacing becomes larger. A second crystallization form of PDP is obtained in which the

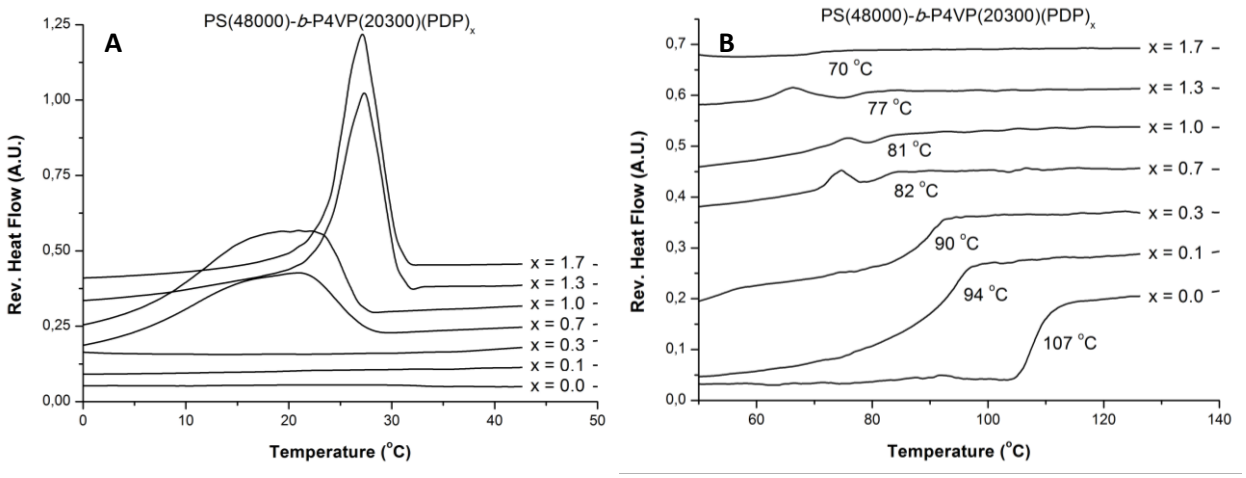

Graph 8. *Normalized modulated DSC stack plots at 3 ˚C/min heating rate of PS(48000)-b-P4VP(20300) with x = 1.70, x = 1.30, x = 1.00, x = 0.70, x = 0.30, x = 0.10, and x = 0.00. The graphs are plotted in reversing heat flow to improve the visibility of the different transitions. (A) At x = 0.7 a melting peak of PDP appears positioned above 20 ˚C which increases in intensity upon going to x = 1.0. At x = 1.3 a new sharp peak appears that is positioned above 25 ˚C and at x = 1.7 the intensity of this peak is slightly higher. (B) Also visible are order-disorder transitions (ODTs), shown as moderate peaks. The T_g of each trace belongs to PS which drops drastically from 107 ˚C for pure PS to 70 ˚C for x = 1.70. These measurements confirm that a fraction of PDP, even at very low concentrations, can migrate into the PS phase, thereby lowering the T_g of PS.*

associated PDP molecules align end-to-end. Furthermore, free PDP is incorporated in these layers with the pyridine heads concentrated in the center.[15] We have shown that for $0.3 < x \leq 1.0$ a PDP melting peak is positioned at 20 ˚C and for $1.0 < x \leq 1.7$ a second larger peak is present positioned at 25 ˚C (Graph 8A). We believe that this observation is in line with the conclusions of Luyten and coworkers and that these two melting peaks indicate the two different crystals of PDP.

To visualize the response of the T_g of PS to the concentration of PDP we plotted the T_g against *x* as is done in Graph 9. Initially the T_g of PS drops steeply with 13 ˚C with increasing concentration of PDP after which the glass-transition drops more steadily. Because of experimental errors in determining the midpoint T_gs of the samples a shift of ±2 ˚C can be expected. The initial drop in the T_g of PS is because PDP acts as a strong plasticizer by increasing the amorphism of PS and is a well-known and studied phenomenon.[16] After this initial drop an increase in the concentration of PDP in PS will cause a further decrease in the T_g. A similar non-linear trend was found by Luyten *et al.* for the T_g of P4VP mixed with PDP.[15]

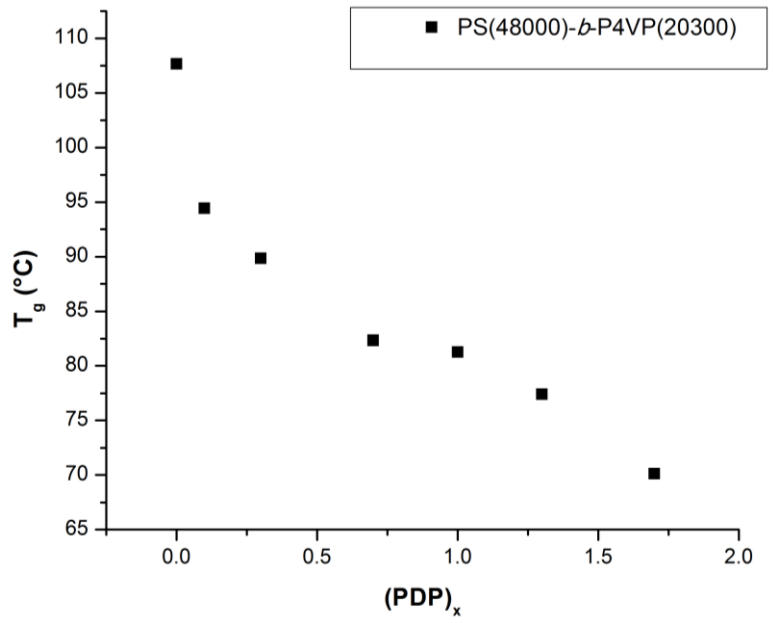

Graph 9. *The glass transition temperature, T_g, plotted against the concentration of PDP, x, for PS(48000)-b-P4VP(20300). The T_g of PS first drops steaply by 13 ˚C after which the drop in T_g decreases slightly which is consistend with literature results.*

2.2.2. *The glass-transition temperature of PS in PS homopolymer mixed with PDP*

We also measured the T_g of PS homopolymer (M_w = 31,000) mixed with PDP with varying concentrations of PDP; 1 wt%, 5 wt%, 10 wt%, 20 wt%, 30 wt%, and 40 wt% at 10 ˚C/min. The molecular weight was chosen such that it was comparable with the molecular weight of PS of the BCP. The results of this experiment are summarized in Graph 10. At low concentrations of PDP there is no melting peak visible of PDP, most probably because the individual PDP molecules are spaced too far apart and cannot crystallize. The T_g of PS at 1 wt% of PDP is already as low as 62 ˚C, drops further to 48 ˚C at 5 wt% and then reaches 38 ˚C at 10 wt% of PDP. When more PDP is added, the melting peak of PDP appears at 20 wt% of PDP at approximately 45 ˚C—20 ˚C higher than the melting temperature of PDP when mixed with PS-*b*-P4VP—and a glass-transition can no longer be distinguished. At a concentration of PDP of 30 wt%, a second higher intensity sharp melting peak appears positioned above 50 ˚C. For 40 wt% both peaks are clearly visible with a higher relative intensity for the first peak. This experiment confirms the suspicion that PDP can migrate into PS and homogeneously mix, where the amphiphile acts as a plasticizer, and lowers the T_g. These effects are more pronounced in the case of the PS homopolymers because in the case of PS-*b*-P4VP PDP will from H-bonds with the

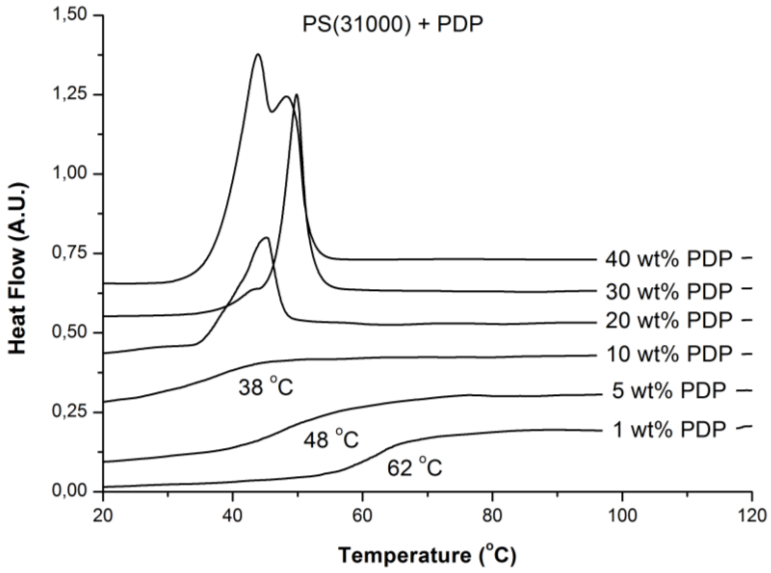

Graph 10. *Normalized stack plot of a DSC scan at 10 ˚C/min heating rate of a PS homopolymer mixed with 1 wt%, 5 wt%, 10 wt%, 20 wt%, 30 wt%, and 40 wt% PDP. The large melting peaks belong to PDP which are not visible at concentrations below 20 wt% PDP. The T_g of PS drops to 62 ˚C at 1 wt% PDP and decreases further to 38 ˚C at 10 wt% PDP. These results confirm that, especially when P4VP is absent, PDP will mix with PS and acts as a plasticizer and thereby lowers the T_g of PS to a large extend.*

pyridine units and, therefore, limiting the amount of PDP that can migrate into PS. Our experiments indicated, however, that especially at higher than stoichiometric amounts of PDP, a small fraction will migrate into PS.

At the basis of these experiments stands the first experiment where PDP was removed by ethanol immersion from PS-*b*-P4VP(PDP)$_{1.0}$. The DSC curves of the pure BCP, the BCP complexed with PDP, and the BCP after the ethanol treatment were measured. It was found that both the T_g of the PS block and the T_g of the P4VP block are fully recovered (i.e., to 105 ˚C and 146 ˚C, respectively) after the immersion in ethanol. We repeated this experiment with two PS homopolymer samples mixed with PDP and the results of this experiment are summarized in Graph 11. The sample containing 20 wt% of PDP before the ethanol treatment shows again the large PDP melting peak at approximately 45˚C which almost completely disappears after the ethanol immersion. It is clear that, since the melting peak is reduced but not completely gone, this indicates that probably not all the PDP is removed from PS. The sample containing 1 wt% PDP before the ethanol treatment differs only slightly from that after ethanol treatment; the T_g is shifted to higher temperatures with only 3 ˚C (and is

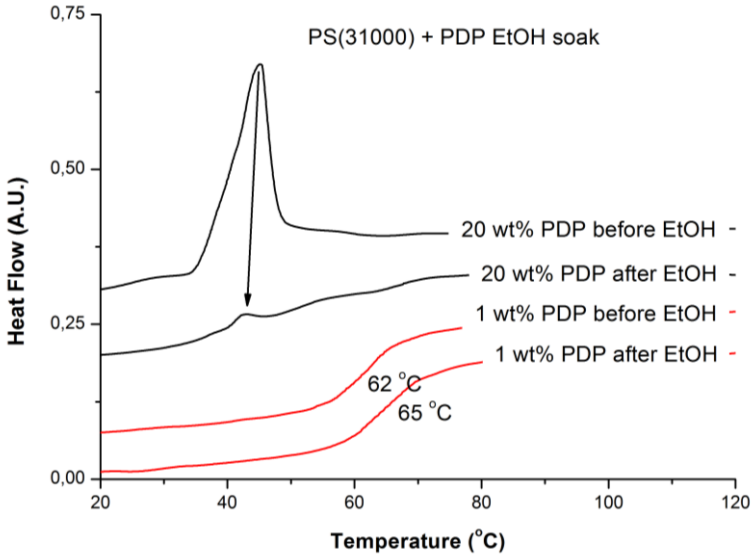

Graph 11. *Normalized stack plot of a DSC scan at 10 ˚C/min heating rate of PS homopolymer mixed with 1 wt% (red) and 20 wt% (black) PDP before and after ethanol immersion to remove PDP. The melting peak of PDP at 20 wt% is reduced but not completely gone after washing with ethanol. At 1 wt% PDP the T_g of PS shits to higher temperatures by only 3 ˚C after ethanol immersion which is possibly an experimental error. This means that only the macro phase separated PDP is (partly) removed and that ethanol is not capable to penetrate inside the PS particles.*

possibly an experimental error). These measurements indicate that PDP is not removed from the PS homopolymer and that only the macrophase separated PDP—visualized by the large melting peak—is (almost completely) washed away. Ethanol is a bad solvent for PS and cannot swell PS, therefore, ethanol cannot penetrate the deeper parts of the particles in order to remove PDP. However, this result cannot be directly compared with the BCP complex situation, because in the BCP, PS is chemically linked to P4VP and ethanol is able to swell the P4VP phase. This means that even though PDP is also mixed with the PS phase in the BCP complex, PDP can still be removed by ethanol through the P4VP phase.

We have, in conclusion, shown that PDP can also be present in the PS phase from which, in the case of the BCP, can be removed again by immersion in ethanol. In the case of PS-*b*-P4VP mixed with PDP we first observe a steep drop of the T_g of PS after which it decreases gradually, which is in agreement with both theory and experiment in literature (see Graph 9). Based on this, we can state that the concentration of PDP, that is present in the PS phase of the BCP, probably remains below 1 wt%. At this concentration the T_g of PS homopolymer was 62 ˚C (Graph 10) whilst the T_g of PS in the

BCP was 70 ˚C at x = 1.70 (Graph 8). We believe that this is direct proof that, even at higher than stoichiometric amounts of PDP, the majority of the PDP is still located at the P4VP phase. A small part can homogeneously mix with the PS phase and, thereby, causing the observed drops in the T_g of PS in the BCP. 1 wt% roughly equals a value of x of 0.012, which would mean that if indeed 1 wt% of PDP migrates into the PS block, instead of measuring x = 1.0 we are actually measuring the supramolecular complex with the composition PS(PDP)$_{0.012}$-*b*-P4VP(PDP)$_{0.988}$. This small error, thus, falls within experimental error that occurs during weighing of the BCP and PDP. It follows that the calculated values of *x* are not a hundred percent accurate. However, because we investigate a large window of the phase diagram of the BCP complex experimentally, the precise knowledge of the concentration of PDP in both of the phases at certain values of *x*, becomes less important.

2.3. Anionic polymerization of PS-b-P4VP

We used the anionic polymerization[17] to obtain the required BCP with the composition PS(31900)-*b*-P4VP(13200) and we analyzed it further by Fourier transform infrared spectroscopy[18] (FTIR), proton nuclear magnetic resonance[19] (^{1}H-NMR) and gel permeation chromatography[20] (GPC), to determine the purity and approximate composition and polydispersity (PDI).

To synthesize our BCP via anionic polymerization we used a high vacuum line that is capable of reaching pressures of 10^{-6} mbar according to literature procedures.[21] At this low pressure we thoroughly cleaned the complete system (i.e., flasks, necks, and tubes) with a high temperature heat gun to remove any volatile impurities. After sufficient cooling down of the flasks we added calcium hydride and subsequently the monomers to allow stirring for three days under a dry nitrogen atmosphere. After this time, styrene turned blue and 4-vinyl pyridine (4VP) yellow. We then condensed both styrene and 4VP to a cleaned (separate) flask containing dibutyl magnesium ($(Bu)_2Mg$) and freshly cut sodium, respectively and stirred overnight under inert atmosphere. After the second drying step styrene turned turbid white and 4VP again yellow (and the sodium brown). Next, we condensed the monomers to a monomer ampoule and applied at least three cycles of freezing, then pumping under high vacuum, followed by thawing (FPT), to remove any air that might be tramped in the monomers (now colorless). We then stored the monomers at -17 ˚C in the dark

until further use. We then cleaned the solvent tetrahydrofuran (THF) by first cooling to below -80 ˚C in an ethanol/liquid nitrogen bath and subsequently added 2 mL of tertiary butyl lithium (tert-BuLi). The initiator generates anions (visible as a bright yellow color) that will react with any impurity that is present in the solvent. We allowed stirring for at least 30-45 minutes and added more tert-BuLi if the color did not persisted. We then let the THF slowly warm up to room temperature (so that the anions slowly terminated and the solution turned colorless) and we subsequently condensed THF to a cleaned flask and applied at least three FPT cycles, with the final thawing under a dry nitrogen atmosphere. In order to make sure that the solvent is clean enough and suitable for anionic polymerization, we first titrated THF at room temperature under stirring with a few drops of secondary butyl lithium (sec-BuLi) which should shortly generate a swirl of yellow color. We then cooled THF to -80 ˚C for 30-45 minutes and slowly added a precisely measured amount of styrene (3.66 ml) with a syringe. Next we initiated the polymerization of PS with sec-BuLi (0.08 ml) and let it react for 30 minutes. After this time we took a 10 mL sample from the reaction mixture and precipitated the PS homopolymer in degassed methanol. After 30 minutes we added a calculated volume of 4VP monomer (1.35 ml) to the reaction mixture and let it react for another 30-45 minutes after which we quenched the reaction with 2 mL of degassed methanol. We collected the BCP by precipitation in water, dried the polymer in a vacuum oven at 60 ˚C for a couple of days, and precipitated the polymer a second time in water from fresh TFH. The BCP was then dried again and analyzed.

In total we used above procedure partly or completely five times to try to synthesize our BCP. However, during the drying of 4VP over sodium it polymerized completely overnight three times and twice a polymeric film was formed that became apparent during condensation. One time this film formed during drying over calcium hydride also. When this film formed we have been able to continue the condensation, however, when the monomer polymerized completely, we were forced to seize the polymerization completely. This could be partly averted by using a tenfold excess of 4VP during the purification so that if some polymerization takes place, some monomer can still be condensed. Furthermore, it is sometimes suggested in literature to stop the purification of 4VP over sodium as soon as yellow discoloration takes place and immediately start the condensation, instead of

stirring overnight over sodium. Two times we were able to purify the monomers and solvent without much problems, but only one time have we been able to obtain a product. However, after the first addition of a calculated volume of initiator to styrene, we did not observe a yellow color, indicating that no initiation had taken place. With the risk that terminated homopolymer of styrene was present in the solvent, we decided to add a second volume of initiator and this time we observed a bright yellow color. After 30 minutes we took a 10 mL aliquot of the reaction mixture and precipitated it in degassed and stirring methanol (with the needle submerged to prevent oxidative coupling). Unfortunately, the yellow solution turned opaque white in the syringe indicating that a reaction occurred with impurities present in the needle. After the second initiation the anionic polymerization continued without any irregularities and after the polymerization of the 4VP block we terminated the reaction with degassed methanol. We next tried to collect the polymer via precipitation in two liters of methanol, however, this resulted in no precipitation and the methanol only turned milky white. Therefore, we ceased the precipitation and were forced to evaporate the methanol under reduced pressure and precipitate again in a different solvent. We precipitated the rest of the THF solution in water to afford a fluffy white solid. The solids that we retrieved from the methanol we precipitated in water also, however, to prevent the incorporation of impurities we did not combine both fractions. We did a second precipitation of the main fraction by re-dissolving it in fresh THF and a second precipitation in water. We then dried the resulting powders in a vacuum oven at 60 ˚C for a couple of days. The polymerization yielded 3,45 grams (0,35 gram + 3,10 gram) of BCP and we obtained 112 milligrams of PS homopolymer. Every attempt to redo this polymerization has thus far failed and, due to time constraints, we were forced to seize our efforts.

We compared the IR spectrum of PS(31900)-*b*-P4VP(13200) with that of the commercial polymer P5154-P4VP, with the same molecular weights of each of the blocks, in an overlay plot as shown in Graph 12. The red line shows some drift in the baseline but the peaks of both spectra overlap and have similar ratios, indicating that both BCPs have the same chemical building blocks; no peaks are observed that are not present in the commercial polymer. We also measured PS(31900)-*b*-P4VP(13200) with ^{1}H-NMR in chloroform and compared the spectrum with that of the commercial counterpart. The result of this comparison is given in Graph 13 which clearly shows that both

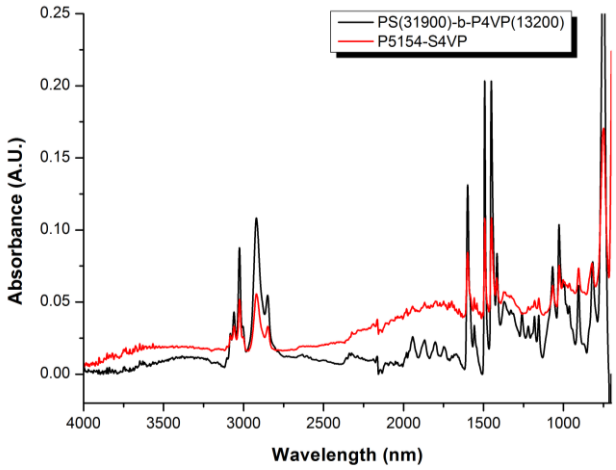

Graph 12. *An overlay infrared spectrum of the synthesized PS(31900)-b-P4VP(13200) via anionic polymerization (black) and the commercial analog P5154-S4VP as supplied by Polymer Source. The red line shows some drift in the baseline but the peaks of both spectra overlap and have similar ratios indicating that both BCPs are similar in composition.*

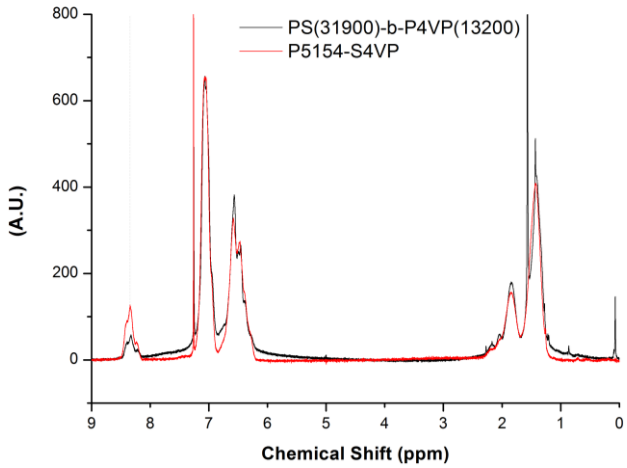

Graph 13. *An overlay ^{1}H-NMR spectrum of the synthesized PS(31900)-b-P4VP(13200) via anionic polymerization (black) and the commercial analog P5154-S4VP (red) as supplied by Polymer Source. Both spectra have identical chemical shifts and the same peak shapes. The only difference is in the area below the peak in the aromatic region belonging to two protons of the pyridine ring which is smaller for the synthesized polymer in the comparison to the commercial polymer. Calculation of the ratios of the peak integrals yielded an approximate polymer composition consisting of 89 mol% PS and 11 mol% P4VP instead of the expected 71 mol% and 29 mol%, respectively. The commercial polymer had a calculated composition of 78 mol% PS and 22 mol% P4VP which is within experimental error of the actual composition.*

polymers have identical chemical shifts and peak shapes (common for polymers). The peak at 0.00 ppm and the peak at 1.57 ppm belong to traces of water and high vacuum grease, respectively, which are present in the polymer and/or in the deuterated chloroform and can be ignored. Furthermore,

there is a small amount of tailing of the peaks that could not be corrected further by the software. The most important dissimilarity between the two spectra is the peak ratio between the three peaks at 8.33 ppm, 7.07 ppm, and 6.57 ppm. The peak at 8.33 corresponds to two protons at the three and five position and the peaks at 7.07 ppm and 6.57 ppm correspond to the two protons at the two and six position of the pyridine ring of P4VP plus five protons of the aromatic ring of PS. From the value of the area below these peaks we can elucidate the ratio between the two blocks in the BCP. We found that for PS(31900)-*b*-P4VP(13200) each P4VP proton has an integral value of 1.33 and each PS proton 10.59. The molar percentage of the PS block can, thus, be calculated via: $100\% \cdot 10.59/(10.59 + 1.33) = 88.8\,\%$ and, therefore, the molar percentage of the P4VP block equals 11.2 %. In comparison, when we do the same calculation for the commercial polymer we find that the molar percentage of the PS block equals 78% and the molar percentage of the P4VP block 22%. The expected molar percentages for PS(31900)-*b*-P4VP(13200) should equal 71% and 29% for PS and P4VP, respectively. However, due to errors in the integration of the peaks and the locking and the shimming of the signal (peak tailing) an error of about 5-10% can be expected. This means that the actual composition of the synthesized PS(31900)-*b*-P4VP(13200) is about 80 mol% PS and 20 mol% P4VP, but still not the aimed 71 mol% and 29% mol%, respectively.

We used GPC to estimate the molecular weight of our BCP. By subtracting the molecular weight of the PS homopolymer of that of the BCP we should be able to determine the molecular weight of the P4VP block and, thus, the approximate composition of the copolymer. However, because appropriate calibration standards do not exist for our BCP, precise analysis of the chemical composition is difficult and, therefore, we must mainly rely on the ^{1}NMR results.[22] The results of the GPC analysis of the PS homopolymer and the PS-*b*-P4VP BCP are summarized in Graph 14. Both samples have been injected twice for reproducibility. The peak at lower retention volumes (i.e., with a higher molecular weight) of the PS homopolymer is caused by oxidative coupling that occurred just before the precipitation (turned opaque white) which results in higher calculated molecular weight of PS. The peak of the BCP is only shifted slightly with respect to the main peak of the PS homopolymer, indicating that side reactions occurred after the addition of the 4VP monomer. In literature lithium chloride (LiCl) is sometimes added in a large access (relative to the later used initiator) to THF to

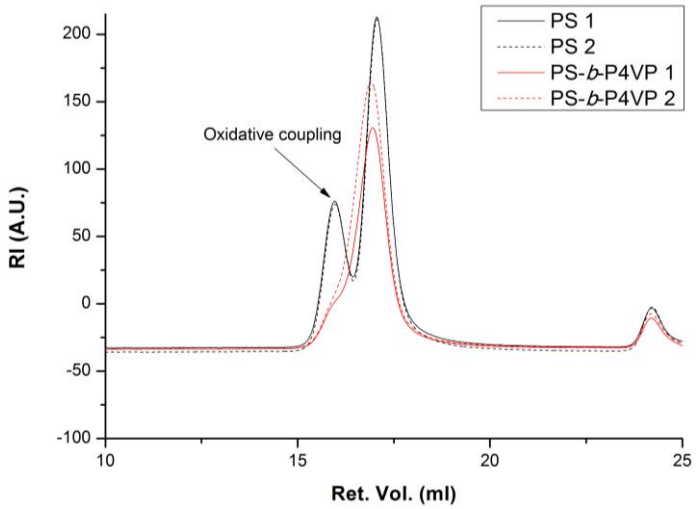

Graph 14. *An overlay GPC trace of the synthesized PS(31900) (black) homopolymer and PS(31900)-b-P4VP(13200) (red) BCP via anionic polymerization, measured in DMF with 0.01 M LiBr and injected twice. The trace of the PS homopolymer shows a peak at lower retention volumes that is an indication that oxidative coupling occurred prior or during precipitation. The traces of the BCP contain a shoulder and, furthermore, are not identical. The maximum of the second injection shows some shift to a higher molecular weight relative to the first injection. Besides the discrepancies between the measurements, the increase in molecular weight of the PS homopolymer after the growth of P4VP is very small. This indicates that the BCP composition that we aimed for is not achieved.*

Table 5. *Calculated results of the GPC analysis of PS(31900) homopolymer and PS(31900)-b-P4VP(13200) BCP synthesized via anionic polymerization.*

Sample	Conc. (g/l)	dn/dc [a] (mL/g)	Mn [b] (g/mol)	Mw [b] (g/mol)	PDI
PS homopolymer 1	1.69	0.1646	47,000	59,000	1.25
PS homopolymer 2	1.69	0.1659	46,000	58,000	1.27
PS(31900)-*b*-P4VP(13200) 1	1.27	-	44,000	59,000	1.33
PS(31900)-*b*-P4VP(13200) 2	1.27	0.1483	47,000	60,000	1.26

[a] *The dc/dc value of the first injection of the BCP gave a unrealistic value and was ignored. Molecular weights were calculated using the dn/dc value of the second injection.* [b] *Values have been rounded up.*

stabilize the anions of the polymerization of P4VP and prevent "back-biting".[23] This might explain why the polymerization did not yield the BCP with the appropriate molecular weight of the P4VP block. Therefore, LiCl should be used in the future to prevent the unwanted back-biting and/or homopolymerization of 4VP. It is probably also required to do the pre-titration of the solvent more thoroughly. The calculated molecular weights are summarized in Table 5 and show almost identical molecular weight and polydispersity of the homopolymer and BCP. The determined molecular weight

of the synthesized BCP was 45,500 g/mol which is in accordance with the calculated molecular weight of 45,000 g/mol. However, the PS homopolymer has the same molecular weight but it is likely overestimated due to the oxidative coupling peak. However, the molecular weight of each peak of the PS homopolymer was estimated to be 46,000 g/mol and 93,000 g/mol for the main peak and the oxidative coupling peak, respectively. Furthermore, the PDI of both the PS homopolymer and the BCP are too high for an anionic polymerization. The PDI of the PS homopolymer is obviously high because of the presence of the oxidative coupling peak. The PDI of the BCP is possibly higher than normal because of some homopolymer that is present, which is manifested as a shoulder at low retention volumes. It, thus, follows that indeed unwanted side reactions (back-biting and/or homopolymerization) occurred, preventing us to obtain the targeted BCP composition.

In order to test whether we made a BCP with appropriate molecular weight of both blocks, to allow microphase separation, we solvent cast two films from the synthesized BCP by mixing it with PDP for x = 1.0. For the first film the amount of PDP was calculated according to the molecular weight of the BCP as we intended to synthesize, thus: PS(31900) and P4VP(13200). The second film contained a PDP concentration for x = 1.0 as calculated according to ^{1}H-NMR analysis, thus: PS-*b*-P4VP with 20 wt% P4VP. We treated both films according to our general procedure and finally determined the morphologies by TEM. For the BCP with the composition with PS(31900) and P4VP(13200), as purchased from Polymer Source, we found a gyroid morphology at x = 1.0, as indicated in Graph 1. The BCP we synthesized, however, indeed did not generate the same result as is unambiguously shown as lamellae for both films in Figure 5. Furthermore, the width of the P4VP phase appears to be small compared to other lamellar morphologies generated in this master's thesis. This is more clear in the right image where we used less PDP than in the left sample. This confirms that indeed the length of the P4VP block is too small as was determined by GPC. Because we do observe lamellae, however, it means that we did obtain a BCP with large enough block lengths to allow microphase separation. Hypothetically speaking, this would suggest that if we add more PDP to this BCP we can obtain the gyroid morphology as well. However, we could of course not use this BCP further for our investigation of the phase behavior of PS-*b*-P4VP(PDP)$_x$.

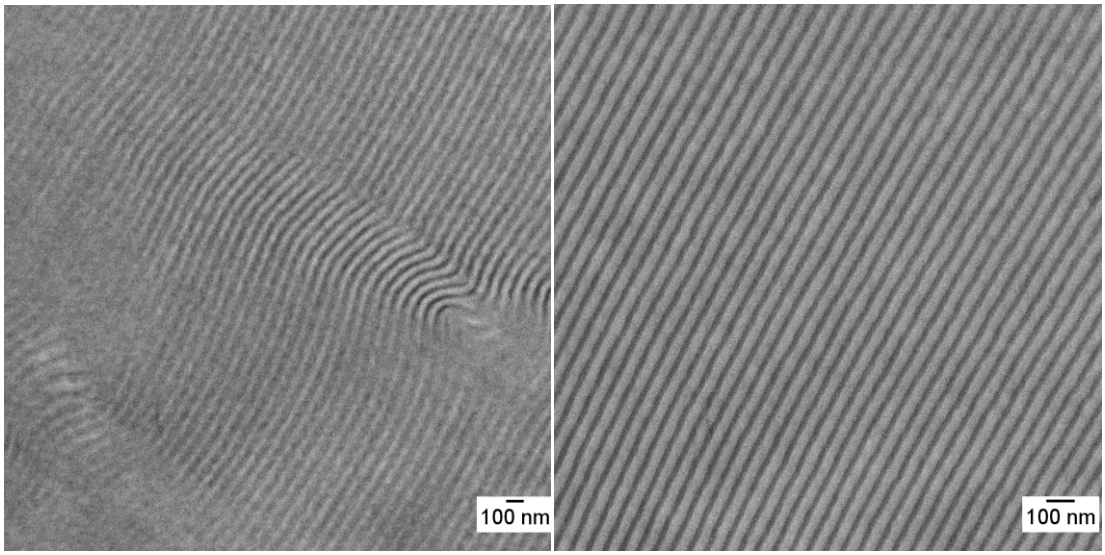

Figure 5. *TEM images of sections of films from the synthesized BCP with x = 1.0 as calculated for a BCP with the composition PS(31900) and P4VP(13200) (left) and with x = 1.0 as calculated for PS-b-P4VP with 20 wt% P4VP (right). The commercial polymer P5154-S4VP, with the same composition as we tried to synthesize, generated a gyroid morphology at x = 1.0. The lamellar morphologies of both films unambiguously show that the targeted composition was indeed not obtained.*

2.4. References

[1] Q. Xu, R.M. Rioux, M.D. Dickey, and G.M. Whitesides, *Accounts of Chemical Research* **2008**, *41*, 1566-1577.

[2] E. Ruska, *The Development of the Electron Microscope and of Electron Microscopy.* Nobel lecture, December 8, 1986.

[3] (a) I.W. Hamley and V. Castelletto, *Prog. Polym. Sci.* **2004**, *29*, 909-948. (b) B. Chu and B.S. Hsiao, *Chem. Rev.* **2001**, *101*, 1727-1761. (c) G.G. Vitale and D.G. LeGrand, *Macromolecules* **1975**, *9*, 749-754.

[4] E.W. Cochran, C.J. Garcia-Cervera, and G.H. Fredrickson, *Macromolecules* **2006**, *39*, 2449-2451.

[5] N.A. Lynd, A.J. Meuler, M.A. Hillmyer, *Progress in Polymer Science* **2008**, *33*, 857-893.

[6] (a) N.A. Lynd and M.A. Hillmyer, *Macromolecules* **2005**, *38*, 8803-8810. (b) Y. Han, J. Cui, and W. Jiang, *Macromolecules* **2008**, *41*, 6239-6245. (c) N.A. Lynd, B.D. Hamilton, and M.A. Hillmyer, *J. Polym. Scie.: part B: Pol. Phys.* **2007**, *45*, 3386-3393.

[7] S. Förster, A. Timman, M. Konrad, C. Schellbach, A. Meyer, S.S. Funari, P. Mulvaney, R. Knott, *J. Phys. Chem. B* **2005**, *109*, 1347-1360.

[8] Th. Zemb, O. Taché, F. Né, and O. Spalla, Rev. Sci. Instrum. **2003**, *74*, 2456-2462.

[9] P. Garstecki and R. Holyst, *J. Chem. Phys.* **2001**, *115*, 1095-1099.

[10] E. Polushkin, G.O.R. Alberda van Ekenstein, M. Knaapila, J. Ruokolainen, M. Torkkeli, R. Serimaa, W. Bras, I. Dolbnya, O. Ikkala, and G. ten Brinke, *Macromolecules* **2001**, *34*, 4917-4922.

[11] (a) W. van Zoelen, T. Asumaa, J. Ruokolainen, O. Ikkala, and G. ten Brinke, *Macromolecules* **2008**, *41*, 3199-3208. (b) W. van Zoelen, E. Polushkin, and G. ten Brinke, *Macromolecules* **2008**, *41*, 8807-8814.

[12] G. Ceccorulli, M. Pizzoli, and M. Scandola, *Macromolecules* **1993**, *26*, 6722-6726.

[13]A.A. van Dooren and B.W. Müller, International Journal of Pharmaceutics **1984**, *20*, 217-233.

[14] I. Vukovic, S. Punzhin, Z. Vukovic, P. Onck, J.T.M. De Hosson, G. ten Brinke, and K. Loos, *ACS Nano* **2011**, *5*, 6339-6348.

[15] M. C. Luyten, G. O. R. Alberda van Ekenstein, G. ten Brinke, J. Ruokolainen, O. Ikkala, M. Torkkeli, and R. Serimaa, *Macromolecules* **1999**, *32*, 4404-4410.

[16] As demonstrated by calculations: (a) T.S. Chow, *Macromolecules* **1979**, *13*, 362-364. (b) P.R. Couchman and F.E. Karasz, *Macromolecules* **1978**, *11*, 117-119. And experimentally: (c) M. Pizzoli, M. Scandola, and G. Ceccorulli, *Eur. Polym. J.* **1987**, *23*, 843-846. (d) M. del Pilar Buera, G. Levi, and M. Karel, *Biotechnol. Prog.* **1992**, *8*, 144-148.

[17] (a) M. Szwarc, *J. Polym. Sci. Part A: Polym. Chem.* **1998**, *36*, ix-xv.(b) J. Smid, M. van Beylen, T.E. Hogen-Esch, *Prog. Polym. Sci.* **2006**, *31*, 1041-1067.

[18] P.Y. Bruice, *Organic Chemistry, Fourth Edition,* pages 499-517. University of California, Santa Barbara, 2004.

[19] P.Y. Bruice, *Organic Chemistry, Fourth Edition,* pages 526-573. University of California, Santa Barbara, 2004.

[20] H.G. Barth, B.E. Boyes, and C. Jackson, *Anal. Chem.* **1996**, *68*, 445R-466R.

[21] (a) G. Gobius du Sart, I. Vukovic, Z. Vukovic, E. Polushkin, P. Hiekkataipala, J. Ruokolainen, K. Loos, and G. ten Brinke, *Macromol. Rapid Commun.* **2010**, *32*, 366-370. (b) G. Gobius du Sart, I. Vukovic, G.O.R. Alberda van Ekenstein, E. Polushkin, K. Loos, and G. ten Brinke, *Macromolecules* **2010**, *43*, 2970-2980.

[22] (a) M.A.R. Meier, S.N.H. Aerts, B.B.P. Staal, M. Rasa, U.S. Schubert, *Macromol. Rapid Commun.* **2005**, *26*, 1918–1924. (b) C.Y. Ryu, J. Han, W. Seok Lyoo, *J. Pol. Scie.: Part B: Pol. Phys.* **2010**, *48*, 2561–2565.

[23] G. Gobius du Sart, 2009. Supramolecular Triblock Copolymer Complexes. Thesis, (PhD) University of Groningen.

3. Conclusions

The phase behavior of the supramolecular complex PS-*b*-P4VP(PDP)$_x$ was extensively studied by TEM and SAXS. The network double gyroid was observed in a number of samples from group I ($0.58 < f_{comb} < 0.62$; $335 < N < 535$; $r \approx 2.5$) and II ($0.61 < f_{comb} < 0.65$; $215 < N < 650$; $r < 2.5$), but was only present as a biphasic morphology with cylinders in group III ($0.61 < f_{comb} < 0.65$; $N = 320$; $r > 2.5$). In group I ($x = 1.0$) the width of the gyroid region decreased (i.e., at a narrower region of volume fractions) with increasing block length (N) of the starting BCP. Furthermore, the size of the gyroid unit cell was ranged from 71 nm to 103 nm. Above a critical value of N the gyroid morphology was no longer observed. In group II the width of the gyroid region was very small and a fluctuation in x of only 0.05 was enough to generate different morphologies. The SAXS data from the samples of group II and group III were, unfortunately, inconclusive—even though some samples showed descent ordering by TEM—and, therefore, we could not confirm the TEM results with SAXS. It is plausible that the used SAXS setup was not suitable for these samples, thus, they should be re-measured on a different setup to rule this out. The results from this work can be used to manufacture porous metal nanofoams. After removal of PDP by ethanol immersion, the porosity of polymer template can be chosen by selecting films with a gyroid morphology from each group. Theoretically, the highest metal nanofoam porosity can be obtained from group II and the lowest from group III. Analysis of glass-transition temperatures by DSC indicated that PDP could also be present in the PS phase at a concentration that was probably below 1 wt%. At this concentration the T_g of PS homopolymer was 62 ˚C whilst the Tg of PS in the BCP was 70 ˚C at x = 1.70 (i.e., 146 wt%). The anionic polymerization technique was applied to synthesize a BCP from group I that was no longer available. Unfortunately, due to numerous setbacks, we have not been able to synthesize the BCP with the composition we aimed for, as was indicated by ^{1}H-NMR and GPC analysis. Films generated from this BCP with $x = 1.0$, indeed did not generate the same result as the commercial polymer (i.e., a lamellar instead of a gyroid morphology).

Future work could include experimental work on the electroless plating of alloys that was briefly discussed in this master's thesis. Furthermore, because we have not been able to successfully apply the anionic polymerization, the procedure should be revised. Another suitable polymerization technique that generates narrow disperse polymers is atom transfer radical polymerization (ATRP).

4. Experimental section

4.1. Materials

Diblock copolymers of polystyrene and poly(4-vinylpyridine) were obtained from Polymer Source Inc. and were used as received. 3-Pentadecylphenol was acquired from Aldrich (98 wt % purity) and was recrystallized twice from petroleum ether. All reagents and solvents were purchased from commercial sources and used without further purification unless otherwise indicated.

4.2. Film preparation

Films of supramolecular complexes of PS-*b*-P4VP with PDP were prepared by homogenizing in chloroform (below 2 wt%) for 24h and subsequently casting in Petri dishes. The Petri dishes were then placed in a larger container with a saturated chloroform vapor atmosphere and chloroform was allowed to evaporate slowly over the course of several days. The films were then placed in a vacuum oven at 30 ˚C for 24h. Next, the films were placed in an oven at 120 ˚C for 4 days at an nitrogen overpressure of 1.5 bar. Finally, the films were allowed to cool down to room temperature. A complete list of the samples that we prepared in this master's thesis is given in Table 3.

4.3. Characterization

The prepared thick films were cut in smaller pieces with a razor blade and embedded in epoxy (Epofix, Electron Microscopy Sciences) and cured at 40 ˚C overnight. Thin sections of 80 nm thick were Microtomed with a Leica Ultracut UCT-ultramicrotome and a Diatome diamond knife at room temperature. The thin sections, floating on water, were next transferred to copper grids. Next, the samples were stained for 45 minutes with iodine. Transmission electron microscopy (TEM) was done on a Philips CM12 transmission electron microscope operating at an accelerating voltage of 120 kV and images were recorded on a Gatan slow-scan CCD camera. Small–angle X–ray scattering (SAXS) was performed in the Nanomicroscopy Center at the Aalto University on a Bruker MICROSTAR microfocus rotating anode X–ray source with Montel Optics (parallel beam, CuKα radiation λ = 1.54

Å), where the beam was further collimated using three sets of JJ X–ray 4–blade slits. A sample–to–detector distance of 4.64 m was used. The scattering intensities were measured using a 2D area detector (BrukerHiStar) and the samples were measured at room temperature in vacuum. (Temperature-modulated) scanning calorimetry (DSC) was performed using a DSC Q1000 (TA Instruments). Samples prepared from the BCP were heated with a rate of 1 °C/min or 3 °C/min, with an oscillation amplitude of 1 °C, and an oscillation period of 60 s. Samples were first equilibrated at -30 °C, heated to 180 °C, cooled to -30 °C, and then heated again to 180 °C. Samples of the homopolymer were scanned in the non-modulating mode and heated with a rate of 10 °C/min. Data were taken from the second heating. ^{1}H-NMR spectra were measured using a Varian AMX400 (400 MHz) instrument at 25 ˚C. Infrared spectra were obtained using a Bruker IFS 88 FTIR spectrometer cooled with liquid nitrogen. Gel permeation chromatography (GPC) measurements were performed in DMF (1 mg mL^{-1}) with 0.01 M LiBr at 70 ˚C (1 mL/min) on a Waters 600 Powerline system, equipped with 2 columns (PL-gel 5 μ, 30 cm mixed-C, Polymer Laboratories) and a Waters 410 differential refractometer. The GPC was calibrated using narrow disperse polystyrene standards (Polymer Laboratories).

4.4. Synthesis

We applied the anionic polymerization technique according to literature procedures.[1] Styrene and 4-vinylpyridine were dried over calcium hydride for 3 days under a dry nitrogen atmosphere and, subsequently, condensed to dibutyl magnesium ($(Bu)_2Mg$) and freshly cut sodium, respectively, and stirred overnight. The monomers were condensed to monomer ampoules and at least three cycles of freezing, then pumping under high vacuum, followed by thawing (FPT) were applied. The monomers were stored at -17 ˚C in the dark until further use. 2 mL of tertiary butyl lithium (tert-BuLi) was then added to tetrahydrofuran (THF) at -80 ˚C to deep yellow that persisted at least 30-45 minutes. THF was subsequently condensed to a cleaned flask and at least three FPT cycles were applied. Next, THF was titrated with a few drops of secondary butyl lithium (sec-BuLi) at room temperature. THF was then cooled to -80 ˚C for 30-45 minutes, styrene added, and initiated with sec-BuLi. After 30 minutes a 10 mL sample was taken from the reaction mixture and precipitated the PS

homopolymer in degassed methanol (to afford a white solid; 112 mg). Next, 4VP was added to the reaction mixture and after 30-45 minutes the reaction was quenched with 2 mL of methanol. The BCP was precipitated in water, collected by filtration, and dried in a vacuum oven at 60 ˚C for a couple of days. The polymer was then precipitated a second time in water from fresh TFH and finally dried to afford a white solid (3,45 g; 73 %). ^{1}H NMR (400 MHz, CDCl3) δ 8.5 – 8.2 (m, 2H), 7.3 – 6.9 (m, 4H), 6.9 – 6.1 (m, 3H), 2.3 – 1.6 (m, 2H), 1.6 – 1.1 (m, 4H). FT-IR (ATR) 3067, 3024, 2917, 2843, 1944, 1879, 1804, 1750, 1654, 1601, 1494, 1451, 1408, 1354, 1247, 1226, 1183, 1151, 1066, 1023, 905, 819, 755 cm^{-1}.

4.5. References

[1] G. Gobius du Sart, 2009. Supramolecular Triblock Copolymer Complexes. Thesis, (PhD) University of Groningen.